

A GAS-RICH NUCLEAR BAR FUELLING A POWERFUL CENTRAL STARBURST IN NGC 2782

SHARDHA JOGEE¹, JEFFREY D. P. KENNEY² & BEVERLY J. SMITH³

Accepted by The Astrophysical Journal

ABSTRACT

We present evidence that the peculiar interacting starburst galaxy NGC 2782 (Arp 215) harbors a gas-rich nuclear stellar bar feeding an M82-class powerful central starburst, from a study based on high resolution interferometric CO (J=1->0) data, optical BVR and H α observations, along with available NIR images, a 5 GHz radio continuum map, and archival HST images. Morphological and kinematic data show that NGC 2782 harbors a clumpy, bar-like CO feature of radius $\sim 7.5''$ (1.3 kpc) which leads a nuclear stellar bar of similar size. The nuclear bar-like CO feature is massive: it contains $\sim 2.5 \times 10^9 M_{\odot}$ of molecular gas, which makes up $\sim 8\%$ of the dynamical mass present within a 1.3 kpc radius. Within the CO bar, emission peaks in two extended clumpy lobes which lie on opposite sides of the nucleus, separated by $\sim 6''$ (1 kpc). Between the CO lobes, in the inner 200 pc radius, resides a powerful central starburst which is forming stars at a rate of 3 to 6 $M_{\odot} \text{ yr}^{-1}$. While circular motions dominate the CO velocity field, the CO lobes show weak bar-like streaming motions on the leading side of the nuclear stellar bar, suggestive of gas inflow. We estimate semi-analytically the gravitational torque from the nuclear stellar bar on the gas, and suggest large gas inflow rates from the CO lobes into the central starburst. These observations, which are amongst the first ones showing a nuclear stellar bar fuelling molecular gas into an intense central starburst, are consistent with simulations and theory which suggest that nuclear bars provide an efficient way of transporting gas closer to the galactic center to fuel central activity. Furthermore, several massive clumps ($10^7 - 10^8 M_{\odot}$) are present at low radii, and dynamical friction might produce further gas inflow. We suggest that the nuclear bar-like molecular gas feature and central activity will be very short-lived, likely disappearing within 5×10^8 years.

Subject headings: galaxies: starburst — galaxies: ISM — galaxies: interactions — ISM: jets and outflows — galaxies: evolution — galaxies: structure

1. INTRODUCTION

In order to drive gas from the outer disk to the nucleus of a spiral galaxy, from scales of tens of kpc to tens of pc, the angular momentum of the gas must be reduced by around six orders of magnitude. It is now accepted that a wide variety of phenomena involving torques and dissipation can drive gas from the outer disk into the circum-nuclear (inner kpc) region. Non-axisymmetric features (Simkin et al. 1980) such as isolated and induced primary bars (Schwarz 1984; Noguchi 1988), as well as tidal interactions and mergers (Negroponte & White 1983; Mihos & Hernquist 1994) can be relevant. However, it is less clear how gas can be driven from scales of kpc to tens of pc. Shocks associated with the primary bar tend to weaken in the inner part of the galaxy and cannot drive further inflow (Shlosman et al. 1989). Numerical simulations (e.g., Combes & Gerin 1985) and observations (e.g., Kenney et al. 1992) show that gas often piles up in rings near inner Lindblad resonances (ILRs). Some studies (e.g., Combes & Gerin 1985) have suggested that gravity torques reverse near ILRs, and thereby stall the transport of gas towards the galactic center. In order to overcome this transport barrier, theory (Shlosman et al. 1989) and simulations (Friedli & Martinet 1993; Combes 1994; Heller & Shlosman 1994) have suggested that nuclear bars nested within a primary bar (or ‘bars within bars’) can be efficient mech-

anisms for driving gas closer to the galactic center to fuel central starbursts and AGNs.

From the observational standpoint, there is mounting evidence from optical and NIR surveys that a large number of galaxies have nuclear stellar bars (Buta & Crocker 1993; Wozniak et al. 1995; Shaw et al. 1995; Elmegreen et al. 1996; Friedli et al. 1996; Jungwiert et al. 1997), and a significant fraction of these galaxies show nuclear activity. However, to date, severely lacking are observations which map the molecular gas in these systems, and show the nuclear stellar bar feeding the gas into a central starburst or AGN. Such observations are highly desirable to constrain formation scenarios and typical lifetimes of nuclear bars, as well as to assess their relative importance with respect to other fuelling mechanisms. The current work presents evidence that the peculiar galaxy NGC 2782 (Arp 215) harbors a massive bar-like molecular feature of radius 1.3 kpc and a similarly-sized nuclear stellar bar which appears to be fuelling molecular gas into the inner 200 pc radius, where resides a powerful central starburst, comparable in intensity to the archetypal starburst M82. This study is based on high resolution ($2''$) interferometric Owens Valley Radio Observatory (OVRO) CO (J=1->0) data, optical observations from the Wisconsin Indiana Yale NOAO (WIYN) telescope, along with NIR images from Engelbracht, Rieke, & Rieke (1999), a 5 GHz radio continuum (RC) map from Saikia et al. (1994), and archival opti-

¹Division of Physics, Mathematics, and Astronomy, MS 105-24, California Institute of Technology, Pasadena, CA 91125

²Yale University Astronomy Department, New Haven, CT 06520-8101

³IPAC/Caltech, Pasadena, CA 91125

cal HST images. This paper is organised as follows. § 2 outlines the previous work done on NGC 2782 and § 3 describes the new observations. § 4.1 presents evidence for a nuclear stellar bar and a possible large-scale primary stellar bar. § 4.2-4.4 present evidence for a nuclear bar-like CO feature of similar size as the nuclear stellar bar, and discuss its kinematics, inclination, and mass fraction. § 4.5 describes the central starburst and how it relates to the nuclear bars. § 4.6 compares the CO bar in NGC 2782 to other systems which host circumnuclear bar-like CO morphologies. § 4.7 discusses the evolution of the circumnuclear region. At what rate is gas being fuelled into the central starburst? How long will the central activity and nuclear bars last? In § 4.8, we compare NGC 2782 to theory and simulations in order to investigate how the nuclear stellar and gas bars formed.

2. PROPERTIES OF NGC 2782 FROM PREVIOUS STUDIES

NGC 2782 (Arp 215), classified as peculiar SAb(rs) (de Vaucouleurs et al. 1991, in RC3) or Sa(s) Peculiar (Sandage & Tammann 1981), is highly suited for addressing numerous astrophysical questions: **(a)** It harbors one of the most luminous circumnuclear starbursts among nearby ($D < 40$ Mpc) spirals (Devereux 1989). The starburst is comparable to the one in M82, with a FIR luminosity of $2 \times 10^{10} L_{\odot}$ (Smith 1991), and a central 10 micron luminosity of $1 \times 10^9 L_{\odot}$ (Giuricin et al. 1994). **(b)** NGC 2782 is both moderately inclined and nearby ($D = 34$ Mpc for H_0 of $75 \text{ km s}^{-1} \text{ Mpc}^{-1}$), and therefore the molecular gas can be resolved on scales of a few hundred parsecs. This is an important advantage over many distant or highly inclined luminous interacting galaxies (e.g., Bryant & Scoville 1999; Evans et al. 1999; Yun et al. 1995) which have been previously mapped in CO. **(c)** The large scale properties (see below) of NGC 2782 suggest it is the product of an intermediate mass-ratio interaction or merger. While minor and major interactions have been widely targeted by both simulations (e.g., Hernquist & Mihos 1995; Barnes & Hernquist 1996) and observations, studies of intermediate mass-ratio interactions/mergers remain comparatively rare.

Large-scale HI and optical properties of NGC 2782: NGC 2782 has a pair of prominent HI and optical tails (Smith 1991; Sandage & Bedke 1994) which bracket an optical disk that harbors three ripples. The eastern tail has been detected in CO (Smith et al. 1999). The R-band image in Fig. 1 (Plate 1) shows the optical disk and tails. Except for the three ripples at radii of $\sim 25''$, $45''$, and $60''$, the optical disk is relatively undisturbed within a radius of $1'$ (10 kpc). The optical disk can be fitted with an exponential surface brightness profile between radii of $\sim 30''$ to $60''$ (e.g., Smith 1994). This shows the galaxy is not as heavily disturbed as major mergers where violent relaxation leads to an $r^{1/4}$ surface brightness profile rather than an exponential one. On the other hand, the presence of the two prominent large-scale HI tails suggests that NGC 2782 is not a minor interaction/merger either. In fact, the optical and HI properties have been modeled by Smith (1994) with an interaction of two disk galaxies which have an intermediate (1:4) mass ratio, and reached closest approach $\sim 2 \times 10^8$ years ago. An alternative possibility is that NGC 2782 is a merger of two disks of unequal

mass.

Circumnuclear properties of NGC 2782: Low resolution H α observations (Hodge & Kennicutt 1983; Smith 1994; Evans et al. 1996) show an unresolved bright region of star formation in the inner $8''$ (1.4 kpc) radius. This region has optical emission spectra (Sakka et al. 1973; Balzano 1983; Kinney et al. 1984) indicative of HII regions, as well as an additional component of highly excited, highly ionised gas which is part of a nuclear outflow (Kennicutt et al. 1989; Boer et al. 1992). Joglee, Kenney, & Smith (1998) hereafter **Paper I**, used optical images, 5 GHz RC data and X-ray data to resolve the inner few kpc into (i) a centrally peaked region of star formation which is elongated east-west with dimensions $\sim 1 \times 1.7$ kpc, (ii) a starburst-driven outflow which forms a well-defined collimated bubble having an extent of ~ 1 kpc, and a closed shell at its edge, as seen in H α , [O III], and 5 GHz RC. While starburst-driven outflows are common, such a remarkable bubble morphology is relatively rare in other starburst galaxies of comparable luminosity. We argued, based on the outflow morphology and timescale of $\sim 4 \times 10^6$ years (Boer et al. 1992), that this outflow is dynamically younger than bi-conical, freely-expanding outflows seen in other starburst galaxies of comparable IR luminosity (e.g., M82). We presented evidence that the outflow is driving hot and warm ionised gas, and possibly cold molecular gas, out of the central kpc of the galaxy.

3. OBSERVATIONS

3.1. CO observations

The central $65''$ of NGC 2782 was observed in the CO ($J=1 \rightarrow 0$) transition at 115.27 GHz with the OVRO millimeter-wave interferometer (Padin et al. 1991) between February and May 1995. The array consists of six 10.4 m telescopes with primary half power beam width of $65''$ at 115 GHz. The galaxy was observed in two array configurations with projected baselines ranging from 15 to 242 m. Data were obtained simultaneously with an analog continuum correlator of bandwidth 1 GHz and a digital spectrometer which is made of four independent modules that each have 32 channels with a velocity resolution of 10.4 km s^{-1} . For our observations, the modules were partially overlapping and covered a total bandwidth of 460 MHz with 116 frequency channels. The passband and flux calibration of the data were carried out using the Owens Valley millimeter array software (Scoville et al. 1993). We corrected for temporal phase variation by observing the phase calibrator 0923+392 every 30 minutes. We corrected for gain variation from one channel to the next across the spectrometer band using spectra of the bright quasars 3C273, 3C84, and 3C345. The absolute flux scale was determined from observations of Uranus, Neptune, and 3C273. We used the NRAO AIPS software to Fourier transform the calibrated uv data and deconvolve the channel maps with the ‘CLEAN’ algorithm as implemented in the AIPS task ‘MX’. We made both uniformly weighted and naturally weighted channel maps. For the uniformly weighted maps, the size of the synthesized beam was $2.1'' \times 1.5''$ ($355 \times 255 \text{ pc}$), at a position angle (PA) of -89.8 deg, the typical r.m.s. noise was 13 mJy per beam, and the peak signal-to-noise was 7. For the naturally weighted maps, the corresponding quantities were

$2.6'' \times 2.0''$ (440×340 pc) at a PA of 89.7° , 10.5 mJy per beam, and 12.5 respectively. The naturally weighted channel maps are shown in Fig. 2. We detect emission above the 3σ level in 35 channels which span velocities ranging from 2365 to 2730 km s $^{-1}$. The naturally weighted maps detect a total flux of 195 Jy km s $^{-1}$ from the central $40''$ (7 kpc) diameter. This corresponds to 73% of the single dish FCRAO flux within $45''$ (Young et al. 1995), and 1.7 times the flux detected in the uniformly weighted channel maps. We combined the clean channels showing emission to make moment 0, 1, and 2 maps, which represent the total intensity, the intensity-weighted velocity field, and the velocity dispersion field respectively.

3.2. Optical observations

We refer the reader to Paper I for the observations and reduction of the optical BVR and H α images taken on the WIYN telescope. For the archival HST images, the original observations were made on April 18, 1997 using the Wide Field Planetary Camera 2 (WFPC2) with a scale of $0.0455''/\text{pix}$. Two exposures of 230 s were taken in each of the broadband F555W and F814W filters, which correspond approximately to the V and I bands respectively. One 600 s exposure and two 1300 s exposures were also taken in the narrowband FR680N filter. This filter is a tunable linear ramp filter, whose central wavelength varies with position across the chip. For these observations, the nucleus of NGC 2782 was placed in the PC chip and the filter was rotated $+15^\circ$ from its nominal position (the FR680P15 mode). With this orientation, the central core of NGC 2782 was observed with an effective central wavelength of 6623\AA and a bandwidth of 86\AA . This band-pass contains the redshifted H α line and the 6584\AA [N II] line of NGC 2782. With this filter, the usable field of view is $\sim 10''$ because of vignetting and cross-talk effects. The images were cleaned of cosmic rays and multiple images in each filter were summed.

4. RESULTS AND DISCUSSION

4.1. The nuclear stellar bar and large-scale oval

Figure 3a shows the I-band image (Smith 1994) with a $2'$ (20 kpc) field of view. The very outermost isophotes are relatively circular, and surround a weak oval feature which has a position angle (PA) of $\sim 20^\circ$ and a radius $\sim 25''$ (4.3 kpc). This oval feature is flanked by two relatively straight dust lanes which are visible in the B and B-V images (Figs. 7a & 7b, Plate 2). The locations of the dust lanes are shown as solid lines in Fig. 3a. The dust lanes appear to extend between radii of $8''$ to $25''$, and are offset towards the leading edge of the large-scale oval feature. The appearance of the dust lanes is similar to the dust lane morphologies observed along the leading edges of primary stellar bars in many spiral galaxies e.g., NGC 1300 (Sandage 1961), NGC 1365 (Teuben et al. 1986). Figure 3b shows the inner $1'$ (10 kpc) diameter of the K-band image from Engelbracht et al. (1999). The uniformly-weighted CO map is superposed as greyscale, and solid lines again mark the locations of the dust lanes. Between the dust lanes, in the inner $7.5''$ (1.3 kpc) radius, the K-band image shows a nuclear oval feature at a PA of $\sim 100^\circ$.

Is the large-scale oval feature of radius ~ 4.3 kpc a pri-

mary bar, and the inner oval of radius ~ 1.3 kpc a nuclear stellar bar? We perform an isophotal analysis of the K-band and I-band images to address this question. The results are shown in Fig. 4, where diamonds and crosses represent the K-band and I-band data respectively: **(a)** The ellipticity profile of the K-band light shows an inner ellipticity maximum (0.28) over which the PA maintains an approximately constant value (100°). Beyond a radius of $\sim 7.5''$ (1.3 kpc), the ellipticity falls to a minimum ($e < 0.1$) and the position angle changes abruptly from 100° to 0 - 10° . **(b)** Between radii of $8''$ to $\sim 25''$ (4.3 kpc), the ellipticity smoothly rises to 0.26 while the position angle twists gradually to a PA of $\sim 20^\circ$. Further out, given the low signal-to noise in the K-band image, we use the I-band image, where the ellipticity falls from 0.26 to below 0.1 in the outer disk, at radii $> 50''$ (8.5 kpc).

The relatively constant position angle (100°) of the nuclear oval and its inner ellipticity maximum (0.28), which is significantly higher than the outer disk's ellipticity (< 0.1), strongly suggest the existence of a nuclear stellar bar of radius $7.5''$ (1.3 kpc). Previous NIR studies (Pompea & Rieke 1990; Forbes et al. 1992) hinted at the existence of this nuclear stellar bar, but it was not as evident because of lower sensitivity and resolution. As further supporting evidence, we note that for a moderately inclined galaxy like NGC 2782, the nuclear oval is unlikely to be caused by projection artifacts which may sometimes emulate a bar (e.g., Friedli et al. 1996; Jungwiert et al. 1997). In addition, the maximum ellipticity (0.28) of the nuclear stellar oval is comparable to the mean maximum ellipticity (0.31) found for the inner cores of other galaxies considered to have nuclear stellar bars (e.g., Friedli et al. 1996). The presence of a nuclear stellar bar is also consistent with the difference between the PA of the nuclear stellar oval, and the PA of the line of nodes, as estimated from the properties of the starburst-driven outflow. The RC bubbles and the H α bubble associated with the outflow (Paper I, also Fig. 3d) suggest a kinematic minor axis of 165° , and for an outflow perpendicular to the disk, this sets the line of nodes at $\sim 75^\circ$. The HST I and V-band images (see § 4.5), more obscured by dust than the K-band image, also reveal stellar and dust lane morphologies consistent with the existence of a nuclear stellar bar.

While the case for a nuclear stellar bar of radius $7.5''$ (1.3 kpc) seems firm, we cannot unambiguously determine if the large-scale oval feature which shows a smooth rise in ellipticity from a radius of $8''$ to $25''$ (4.3 kpc) is a primary bar. On one hand, the relatively straight and prominent dust lanes (described above) associated with the leading edge of the large-scale oval are strongly reminiscent of primary stellar bars. On the other hand, we note that within the large-scale oval, between radii of $8''$ to $25''$, the PA of the I-band isophotes is not constant, but twists. A constant position angle would have clinched the case for a primary bar, but isophotal twist neither proves nor excludes the presence of a primary bar. In general, spiral arms, dust lanes, a radius-dependent triaxiality associated with a primary bar or/and a bulge, as well as intrinsically misaligned isophotal surfaces not associated with a primary bar, may all produce isophotal twist (Wozniak et al. 1995; Jungwiert et al. 1997). In the case of NGC 2782, we can exclude spiral arms or ripples as the cause of the ob-

served isophotal twist, since such features are not present between radii of $8''$ to $25''$ in the K-band or I-band image (Figs. 3a-b). (The ripples in the I-band image exist only further out, at radii of $\sim 25''$, $45''$, and $60''$). However, since dust and other causes of isophotal twist cannot be excluded, a firm case cannot be made for a primary stellar bar. In summary, we hence conclude that NGC 2782 harbors a nuclear stellar bar of radius $7.5''$ (1.3 kpc), which is nested within a large-scale oval of radius $25''$ (4.3 kpc), which may be, but is not necessarily, a primary bar.

4.2. The circumnuclear CO morphology and kinematics

The previously published low resolution ($6''$ or 1 kpc) CO ($J=1\rightarrow 0$) Nobeyama Millimeter Array (NMA) map (Ishizuki 1994) shows an elongated feature with two barely resolved CO peaks in the inner $9''$ (1.5 kpc) radius, and fainter emission further out. The data gave limited additional information on the distribution and kinematics of the gas in the inner few kpc. Our high resolution ($2.1'' \times 1.5''$ or 355×255 pc) OVRO CO ($J=1\rightarrow 0$) map in Fig. 5a shows a bar-like CO feature of radius $\sim 7.5''$ (1.3 kpc), and resolves it into two extended, clumpy lobes which lie on opposite sides of the nucleus, separated by $\sim 6''$ (1 kpc). Between the two CO lobes, in the inner 200 pc radius, the starburst activity peaks sharply (Paper I & § 4.5). It is possible that the CO depression between the lobes is the result of gas consumption by star formation or/and gas blown out in the starburst-driven wind. The bar-like CO feature has a similar size as the nuclear stellar bar of radius $7.5''$ (1.3 kpc) and PA ~ 100 deg identified in § 4.1. The two CO lobes lie on the leading edges of this nuclear stellar bar, assuming a clockwise sense of rotation for the stellar bar. (This sense of rotation for the stars stems from the assumption that they are rotating in the same sense as the molecular gas, for which we infer a clockwise sense of rotation from the kinematics). Gas on the leading edges of a stellar bar is expected to lose angular momentum and be driven inwards, as a result of shocks and gravitational torques exerted by the stars on the gas (e.g., Schwarz 1984; Combes & Gerin 1985; Athanassoula 1992; Friedli & Martinet 1993; Byrd et al 1994; Piner et al. 1995). It is thus possible that the nuclear stellar bar is fuelling gas from the CO lobes into the central starburst.

The intensity-weighted CO velocity field shown in Fig. 5b provides further insight into the circumnuclear dynamics. No significant sign of warping is seen: there is no conspicuous distortion of the kinematic principal axes into S-shapes over the inner $8''$ (1.4 kpc) radius, and the PA of the CO kinematic minor axis (KMNA) is consistent with PA (165 deg) of the minor axis suggested by the starburst-driven RC and H α outflow bubbles (Paper I & Fig. 3d). Most of the isovelocity contours in the central $8''$ (1.4 kpc) radius form a ‘spider-diagram’, suggesting that circular motions are important. The CO velocity field, with red-shifted velocities lying to the west of the kinematic center, implies a clockwise sense of rotation for the circumnuclear molecular gas if we assume the near side of the galactic disk lies to the north. This orientation for the galactic disk was inferred in Paper I from the morphology of the starburst-driven outflow and the dust lanes (see also § 4.3). The circumnuclear CO velocities are consistent with the previously observed kinematics of the cores of HI (Smith 1994) and ionised (Boer et al. 1992) gas. However, su-

perposed on the predominantly circular velocity field, are non-circular motions in several regions, particularly near the CO lobes. The kinematic major axis (KMJA) is at ~ 75 deg near the center, but it curves near the eastern and western CO lobes. This suggests bar-like streaming motions in the CO lobes.

The CO spatial velocity plot along the KMJA, shown in Fig. 6a, probes the gas kinematics in more detail. The spatial velocity plot has a width of $\pm 1''$ about the KMNA, and the systemic velocity of 2550 km s^{-1} has been subtracted from the velocities shown on the y-axis. On the eastern side of the major axis, between $1''$ and $4''$, complex kinematics and an apparent gap in the spatial-velocity plot at a velocity of -50 km s^{-1} are seen. The features marked as A1, A2, A3, and A4 in Fig. 6a delineate large linewidths at the position of the western and main eastern CO peaks. Notice also that the observed velocities increase rapidly between the center and A3, but the ‘rotation curve’ become shallow as it goes through the western CO peak. What is producing the complex kinematics in the CO peaks? These kinematics may be the manifestation of bar-like azimuthal streaming motions and radial inflow motions which are expected in gas lying on the leading edges of a nuclear stellar bar. It is difficult to directly identify a radial inflow component in the data because the observed line of sight velocity is in general a combination of several velocity components which cannot be easily disentangled from each other: azimuthal in-plane motions, vertical out-of-plane motions, and radial in-plane motions (Eq. 8-60 in Mihalas & Binney 1981). In the case of NGC 2782, spatial velocity cuts which go through the CO peaks are close to the KMJA, and hence are more sensitive to azimuthal in-plane and vertical out-of-plane motions than to radial in-plane motions.

We also point out that some molecular gas might be outflowing from the starburst region. The CO intensity map in Fig. 5a shows two CO spurs (labelled O1 and O2) between the CO lobes. The CO isovelocity contours in Fig. 5b show clear kinks at the base of these spurs, indicating deviations from circular motions. Fig. 3d shows that these spurs lie just north and south of the central starburst region, and are elongated along the CO KMNA (165 deg), within the two RC outflow bubbles. In Fig. 6b, the spatial-velocity plot along the KMNA shows that gas velocities deviate from the systemic velocity (2555 km s^{-1}) by $\sim (+30 \text{ km s}^{-1})$ in the northern spur, and by $\sim (-30 \text{ km s}^{-1})$ in the southern spur. With the near side of the disk being north (Paper I & § 4.5), these velocities are consistent with vertical out-of-plane motions or radial in-plane motions. Although we cannot strictly distinguish between the two possibilities, the location of the spurs with respect to the central starburst and outflow bubbles, and their elongation along the KMNA provide circumstantial support for outflowing gas.

4.3. The inclination of the circumnuclear molecular gas

We need to estimate the inclination of the circumnuclear molecular gas in order to subsequently constrain properties such as the molecular gas mass fraction and kinematics. We first note that the CO velocity field (Fig. 5b) does not suggest any significant warping, and therefore it is reasonable to assume that the circumnuclear molecular gas lies in one plane. We infer that the inclination (i_{co}) of

this plane is ~ 30 deg, from the following arguments: (i) We can rule out an inclination close to edge-on because it would imply that the large thickness of the observed bar-like CO distribution corresponds to unrealistically large scale heights (~ 1 kpc) for molecular gas *throughout the region* between radii of $3''$ (510 pc) to $7.5''$ (1.3 kpc). While one might conceivably justify large scale heights in the central $2''$ (340 pc) radius where intense starburst activity and winds prevail, it would be difficult to account for such large scale heights out to a radius of 1.3 kpc. (ii) The Tully Fisher relation for optical blue magnitudes requires $i_{\text{co}} > 25$ deg in order to ensure that the peak CO rotational speed ($165 \text{ km s}^{-1}/\sin i_{\text{co}}$) does not exceed the maximum rotational speed of 400 km s^{-1} (Rubin et al. 1985) observed in peculiar and normal galaxies which are optically as bright or brighter than NGC 2782. We can also apply the infrared Tully Fisher relation between the H magnitude (m_{H}) and the peak rotational speed (V_{max}), [$m_{\text{H}} = 2 - \log V_{\text{max}}$] (Pierce & Tully 1988). Assuming $m_{\text{H}} = 10.1$ (de Vaucouleurs & Longo 1988), and an uncertainty of 0.7 magnitude in the Tully Fisher relation, we find that i_{co} is (31 ± 6) deg. (iii) This moderate value of ~ 30 deg we estimated for i_{co} is consistent with the inclination of dust in the inner few kpc, as constrained by properties of the starburst-driven outflow. The 5 GHz RC image shows kpc-sized outflow bubbles *both* north and south of the nucleus, while only the southern bubble is visible in the optical H α and [O III] images (see Paper I). This suggests that the northern bubble is obscured by dust in the inner few kpc of a moderately inclined disk whose near side lies to the north (Jogee et al. 1998). (iv) Based on the relatively undisturbed appearance of the outer disk (Fig. 1; Plate 1) within a radius of $1'$ (10 kpc), one expects its inclination to be similar to i_{co} . It is reassuring to note that the outermost isophotes of the I-band image (Fig. 3a & 4) do indeed suggest an inclination of ~ 30 deg for the outer disk.

How do the nuclear stellar bar and the bar-like CO feature in the inner $7.5''$ (1.3 kpc) radius relate to the large-scale features in NGC 2782? The naturally weighted OVRO CO map is overlaid on the B-V image in Fig 7b. (Plate 2). The bar-like CO feature of radius $7.5''$ (1.3 kpc) contains 75 % of the total CO emission detected within the central $20''$ (3.4 kpc) radius. Two faint CO streams stem from the western and eastern ends of the CO bar and extend out in a northeast and southwest direction. The southern CO stream suggests a very loosely wound spiral arm. In Fig 7b. (Plate 2), it is significant and striking that the CO streams tend to lie along the two relatively straight dust lanes in the B-V image. As described in § 4.1, these dust lanes are offset towards the leading edge of the large-scale stellar oval of radius $25''$ (4.3 kpc), which might be a primary stellar bar. Prominent dust lanes along the leading edges of a stellar bar trace the loci of shocks which cause bar-driven gas inflow (e.g., Tubbs 1982; Schwarz 1984; Combes & Gerin 1985; Athanassoula 1992; Byrd et al 1994; Piner et al. 1995). It is therefore likely that the CO streams represent the gas still inflowing towards the CN region under the action of the large-scale stellar oval.

4.4. How massive is the bar-like molecular feature?

The mass and dynamical mass fraction of the bar-like CO feature are important for differentiating between scenarios for the formation of nuclear bars (§ 4.8), and for predicting how the circumnuclear region will evolve (§ 4.7). We estimate the mass of molecular hydrogen (M_{H_2}) from the relation (Kenney & Young 1989; Scoville & Sanders 1987) :

$$\frac{M_{\text{H}_2}}{(M_{\odot})} = 1.1 \times 10^4 \left(\frac{\chi}{2.8 \times 10^{20}} \right) (D^2) \left(\int S_{\text{CO}} dV \right) \quad (1)$$

where D is the distance in Mpc, $\int S_{\text{CO}} dV$ is the integrated line flux in Jy km s^{-1} , and χ is the CO-H $_2$ conversion factor (defined as the ratio of the beam-averaged column density of hydrogen to the integrated CO brightness temperature). Is the Milky Way value of $2.8 \times 10^{20} \text{ H}_2 \text{ cm}^{-2} (\text{K km s}^{-1})^{-1}$ appropriate for χ in a circumnuclear starburst region, where molecular gas might not be in virial equilibrium, and the gas temperature T and density ρ can be significantly higher than in Milky Way clouds? Since χ depends on $\sqrt{\rho}/T$ (Scoville & Sanders 1987), one might argue that the effects of elevated temperatures and densities will partially offset each other. On the other hand, multiple-line studies and radiative transfer models (Wall & Jaffe 1990; Wild et al. 1992; Helfer & Blitz 1993; Aalto et al. 1995) have suggested that χ is lower than the Milky Way value by a factor of ~ 3 in the centers of some starburst galaxies. Given the absence of multiple-line studies in NGC 2782, we cannot determine if χ deviates significantly from the Milky Way value, and we therefore choose to express many results in this paper explicitly in terms of χ_1 , where $\chi_1 = (\chi/2.8 \times 10^{20})$.

The hydrogen mass (M_{H_2}) in the central $20''$ (3.4 kpc) radius is $\sim (2.4 \times 10^9 \chi_1) M_{\odot}$. The total mass of molecular gas including the contribution of He is $\sim (3.3 \times 10^9 \chi_1) M_{\odot}$, assuming a solar composition. About 75 % or $(2.5 \times 10^9 \chi_1) M_{\odot}$ of this gas lies in the bar-like CO feature of radius $7.5''$ (1.3 kpc). The bar-like molecular feature is therefore quite massive if χ_1 is not significantly less than 1. The dynamical mass enclosed within the radius ($\sim 7.5''$ or 1.3 kpc) of the nuclear stellar bar is $(8 \times 10^9 / \sin^2 i_{\text{co}}) M_{\odot}$. This value is derived assuming a flat rotational speed of $(165 \text{ km s}^{-1}/\sin i_{\text{co}})$ from the CO velocity field, where i_{co} is the inclination of the circumnuclear molecular gas. The molecular gas $(2.5 \times 10^9 \chi_1 M_{\odot})$ therefore makes up $(30 \% \sin^2 i_{\text{co}} \chi_1)$ of the dynamical mass. With $i_{\text{co}} \sim 30$ deg (§ 4.3), the gas mass fraction is $(7.5 \chi_1) \%$.

4.5. Circumnuclear star formation and dust morphologies

The H α and [O III] observations presented in Paper I show that star formation in the disk of NGC 2782 is concentrated in the bar-like CO feature of radius $7.5''$ (1.3 kpc) and along the ripple located at $\sim 25''$ (4.3 kpc). We estimate the SFR in the CO bar from NIR data rather than optical tracers in order to reduce extinction problems. Using the Br γ luminosity ($1.6 \times 10^{10} L_{\odot}$; Puxley et al. 1990) in the central $10''$ (1.7 kpc) radius, and assuming a case B recombination with an electron density n_e of 10^4 cm^{-3} , a temperature of 10^4 K , and an extended Miller-Scalo IMF (Kennicutt 1983), we derive a SFR of $5\text{--}6 M_{\odot} \text{ yr}^{-1}$. An alternative estimate of the SFR can be obtained

by assuming that the total FIR luminosity ($2 \times 10^{10} L_{\odot}$; Smith 1991) originates predominantly from dust heated by massive stars in the circumnuclear region. Applying the method described by Hunter et al. (1986) then gives a SFR of $\sim 4/\beta M_{\odot} \text{ yr}^{-1}$, where β represents the ratio of the FIR luminosity to the total bolometric luminosity of the massive stars. For β between 0.5 and 1, the circumnuclear SFR lies between 4 to $8 M_{\odot} \text{ yr}^{-1}$. Star formation is happening throughout the bar-like CO feature, but it is mostly concentrated between the CO lobes in central 200 pc radius, as seen in both H α and 5 GHz RC (Fig. 3d). This central starburst has a SFR of 3 to $6 M_{\odot} \text{ yr}^{-1}$, comparable to the powerful archetypal starburst M82.

Fig. 8 shows the HST H α + [N II] image with a $10''$ usable field of view. The HST image reveals a wealth of details within features which were previously identified in ground-based images. The southern outflow ‘bubble’ (Jogee et al. 1998) is clearly resolved, while knots of HII regions stand out in the arc of star formation which lies north of the central starburst and extends approximately east-west. The HST V-band (F555W) with a $35''$ (6 kpc) field of view is shown in Fig. 9a. The uniformly weighted ($2.1'' \times 1.5''$ or 355×255 pc) CO map is superposed as contours on the V image in Fig. 9b. Figs. 9a-b show the northern arc of star formation and reveal conspicuous dust lanes which stem from the western end of the arc and extend northeast out to a radius of $25''$ (4.3 kpc). These dust lanes coincide with those seen in the ground-based B-V image (Fig. 7a; Plate L2), offset towards the leading edge of the large-scale stellar oval shown in Fig. 3a. Furthermore, very striking in Fig. 9a but not evident in ground-based images, are dust lanes running approximately east-west, about $4''$ (680 pc) north of the nucleus. These nuclear dust lanes, are offset in a leading sense with respect to the nuclear CO and stellar bars, and could represent shocks associated with these nuclear bars. The fact that these dust lanes are conspicuous to the north of the nucleus, but not to the south, supports our contention (Paper I) that the northern side of the inner disk is the near side.

4.6. The nuclear CO bar in NGC 2782 compared to other systems

While a stellar bar can be defined in terms of periodic families of stellar orbits, there is no firm definition of what constitutes a gas bar since gas, being collisional and dissipative, does not follow closed periodic orbits, especially crossing orbits. In the literature, gas distributions which are observed to be elongated, double peaked, or double-lobed have all been loosely called ‘gas bars’. It is therefore important to characterise how the bar-like CO feature in NGC 2782 differs from other bar-like circumnuclear CO morphologies:

(i) *Highly inclined systems*: A high inclination as well as low resolution CO data makes it ambiguous whether a bar-like CO morphology is a molecular bar or a relatively axisymmetric gas ring viewed edge-on. The nearly edge-on minor mergers NGC 2146 and NGC 3079 are two typical examples. CO observations of NGC 3079 at $4''$ (300 pc) resolution (Irwin & Sofue 1992) show a centrally peaked elongated component of radius ~ 800 pc. In NGC 2146, $7''$ (700 pc) resolution CO observations show strong CO emission from two lobes which lie ~ 1 kpc apart (Jackson & Ho 1988; Young et al. 1988). However, the double-

lobed CO morphology in NGC 2782 is unlikely to be the result of a high inclination. The CO map in Fig. 5a is not suggestive of a highly inclined ring, and we have already presented several arguments for a moderate inclination (30 deg) rather than an edge-on inclination in § 4.3. Hence, NGC 2782 likely has an *intrinsically* bar-like, non-axisymmetric gas distribution in the galactic plane.

(ii) *Gas concentrations near ILRs in galaxies without a nuclear stellar bar*: A bar-like double-peaked CO morphology in the moderately inclined galaxy NGC 6951 has been interpreted as gas piling up near inner Lindblad resonances (Kenney et al. 1992). Several differences demarcate NGC 2782 from NGC 6951. While the star formation in NGC 6951 peaks in a ring-like configuration near the ILRs, the star formation in NGC 2782 peaks sharply *in the central 200 pc, interior to the two CO lobes*. This suggests that in the recent past of NGC 2782, gas must have reached the central starburst in the inner 200 pc. There is no published evidence for a nuclear stellar bar in NGC 6951, and the CO peaks lie near the turnover point of the rotation curve. On the other hand, NGC 2782 hosts a kpc-sized nuclear stellar bar, and the CO lobes *lie on the leading edges of this nuclear stellar bar*, well inside the turnover radius ($\sim 6''$ or 1 kpc) of the rotation curve, and show bar-like streaming motions (§ 4.2). This suggests that while in NGC 6951 gas may be piling up near ILRs, in NGC 2782 it may be experiencing further inflow from the CO lobes into the central starburst, likely under the action of the nuclear stellar bar. In fact, the formation of a nuclear stellar bar might be a way of converting non-starbursts like NGC 3351 and NGC 6951 into centrally concentrated starbursts like NGC 4102, NGC 4536, NGC 3504, and NGC 470 (Jogee 1998; Jogee & Kenney 1998).

(iii) *Other systems with potential nuclear gas bars*: Nuclear stellar bars observed to date (Elmegreen et al. 1996; Friedli et al. 1996; Jungwiert et al. 1997) have a radius ranging from a few hundred pc to a kpc. High resolution interferometric CO observations needed to identify any bar-like molecular counterpart are not available in many cases such as NGC 1097, NGC 5850, and NGC 3981. A similar case is NGC 7552 where K-band and H_2 S(1) 2.12 μm images (Schinnerer et al. 1997) show an oval feature of radius $\sim 5''$ (500 pc). In other galaxies such as Maffei 2 (Hurt & Turner 1991) and IC342 (Ishizuki et al. 1990) CO observations show elongated bar-like CO distributions in the inner 500 pc radius, but there is no conclusive evidence for a nuclear stellar bar.

In the case of M100 (NGC 4321), both high resolution CO and NIR data exist, but differing model-dependent interpretations have been proposed. NIR images of M100 (Knapen et al. 1995a) show a stellar oval of radius $4''$ (320 pc), offset by only 4 deg from a large-scale stellar bar of radius $60''$ (5 kpc). CO maps (Rand 1995; Garcia-Burillo et al. 1998) show two trailing molecular gas spiral arms which extend from a gas concentration in the central $\sim 1.5''$ (100 pc) radius. Numerical models of Garcia-Burillo et al. (1998) suggest that M100 harbors a fast-rotating nuclear stellar bar nested within a large-scale bar, while models of Knapen et al. (1995b) suggest that a single large-scale bar exists.

4.7. The evolution of the circumnuclear region

There exists few direct observational studies of how the circumnuclear region evolves under the impact of a nuclear stellar bar. We address this issue in NGC 2782 where we have concurrent observations which reveal the distribution of molecular gas and star formation in the region of the nuclear stellar bar. We emphasise that given the complexity of the interplay, the ensuing discussion should be taken in a qualitative sense.

4.7.1. The gravitational torque exerted by the nuclear stellar bar

The nuclear gas bar is offset towards the leading edge of the nuclear stellar bar (§ 4.2). We therefore expect the gravitational torque exerted by the nuclear stellar bar on the gas bar to remove angular momentum from the gas. The net radial inflow rate cannot be directly measured for several reasons. The galaxy is relatively face-on ($i < 30$ deg) and hence the line-of-sight velocities are not very sensitive to in-plane azimuthal and radial velocities. Furthermore, along a general position angle, the line-of-sight velocity is made up of a combination of in-plane azimuthal and radial motions, and out-of-plane vertical motions. It is easiest to isolate the in-plane radial component along the kinematic minor axis where the in-plane azimuthal motions are negligible. However, the nuclear stellar bar along which one might expect radial gas inflow is at a very different PA (100-110 deg) from the kinematic minor axis (165 deg). This orientation makes the direct observation of the radial component difficult. We therefore adopt a semi-empirical method where we try to estimate the torque from the data, and hence derive the radial component of the velocity at different positions.

In the ensuing discussion, we use unit position vectors (\mathbf{e}_r , \mathbf{e}_θ , \mathbf{e}_z) to describe the circumnuclear region of the galaxy, and Φ to describe the stellar potential. The unit vector \mathbf{e}_z is perpendicular to the plane of the nuclear stellar bar, (\mathbf{e}_r , \mathbf{e}_θ) are in the plane of the bar, and the angle θ is measured w.r.t. the major axis of the nuclear stellar bar. The torque per unit gas mass exerted by the nuclear stellar bar on a gas element at a position (r , θ) is :

$$\tau = \frac{\partial \Phi}{\partial \theta} \mathbf{e}_z - r \frac{\partial \Phi}{\partial r} \mathbf{e}_\theta \quad (2)$$

Gas shocked on the leading edge of the nuclear stellar bar loses angular momentum per unit gas mass (L_z) at the rate :

$$\frac{dL_z}{dt} \mathbf{e}_z \approx 2 r \Omega_s \frac{dr}{dt} \mathbf{e}_z \quad (3)$$

where Ω_s is the pattern speed of the secondary bar. Since $d\mathbf{L}/dt = \tau$, the radial velocity is given by,

$$\frac{dr}{dt} \approx \frac{1}{2 r \Omega_s} \frac{d\Phi}{d\theta} \quad (4)$$

The expression we derived for the radial velocity dr/dt in Eq. 4 is consistent with the one given by Quillen et al. (1995). The term involving Φ in the above equation can be evaluated in several ways. One method is to convolve the K-band image to obtain the barred stellar potential (e.g., see Quillen et al. 1995). This method requires detailed

modeling and knowledge of the mass-to-light ratio in the region of the stellar bar. In the circumnuclear starburst region of NGC 2782, the mass-to-light ratio is uncertain. We therefore adopt a different, albeit more simplistic approach. We approximate the potential of the nuclear stellar bar with an analytic expression for a barred logarithmic potential (Binney & Tremaine 1987):

$$\Phi(r, \theta) = \frac{V_o^2}{2} \ln [R_c^2 + r^2(\cos^2\theta + \frac{\sin^2\theta}{q^2})] \quad (5)$$

In the above expression, R_c is a core radius, q is the axial ratio, and V_o is a circular speed. Using Eq. 4, the radial velocity dr/dt is then :

$$\frac{dr}{dt} \approx \frac{V_o^2 r}{4\Omega_s} \sin 2\theta \left[\frac{(1/q^2 - 1)}{R_c^2 + r^2(\cos^2\theta + \sin^2\theta/q^2)} \right] \quad (6)$$

It is noteworthy that for radii $r \gg R_c$, the radial velocity is highly sensitive to the term $(\sin 2\theta/\Omega_s r)$. This dependence correctly predicts that gas elements on the minor axis of the nuclear stellar bar (where $\theta = 90$ deg, 270 deg), will experience no net radial inflow. Furthermore, nuclear gas bars which are offset by relatively large angles (e.g., 45 deg) with respect to the nuclear stellar bar major axis will be rapidly driven inwards. This suggestion is consistent with simulations (e.g., Friedli & Martinet 1993), where the nuclear gas bar is observed to lead the nuclear stellar bar only by a small angle of order 5 to 10 deg.

In order to estimate the radial velocity for NGC 2782, the constants Ω_s , V_o , and q must be evaluated. The pattern speed (Ω_s) of the nuclear stellar bar is estimated by assuming that the corotation resonance of the nuclear stellar bar is near the radius ($\sim 8''$ or 1.4 kpc) of the ellipticity minimum in Fig. 4. The condition $[\Omega = \Omega_s]$, where Ω is the angular speed, leads to $\Omega_s \sim (123 \text{ km s}^{-1} \text{ kpc}^{-1} / \sin i_{co})$. With $i_{co} \sim 30$ deg (§ 4.3), the nuclear bar pattern speed is $\sim 245 \text{ km s}^{-1} \text{ kpc}^{-1}$, corresponding to a rotation period of $\sim 3 \times 10^7$ years. In order to determine V_o , we note that in the limit $r \gg R_c$ and $q=1$, the potential Φ produces a flat rotation curve with speed V_o . For NGC 2782, we assume that the turnover velocity of ($165 \text{ km s}^{-1} / \sin i_{co}$) given by the CO kinematics (§ 4.2) is a good approximation for V_o . With $i_{co} = 30$ deg, $V_o \sim 330 \text{ km s}^{-1}$. We adopt an axial ratio $q \sim 0.85$ since the ellipticity of the nuclear stellar bar in the K-band light is 0.28 , and the stellar potential will have a lower ellipticity since it is a convolution of the density profile. Near the bar end, at a radius $r \sim 6''$ (1 kpc), gas elements located at $\theta \sim 5$ - 20 deg from the stellar bar in NGC 2782 have radial velocities of ~ 15 - 45 km s^{-1} . It is important to realise that the local radial velocity (15 - 45 km s^{-1}) is not necessarily equal to the net radial mass inflow velocity. This is because the net inflow rate depends on the radial inflow velocity at *all* parts of the gas orbit, and not only when it is on the leading edge of the bar. The true average mass inflow velocity is probably lower. The bar-like CO feature contains $\sim 2.5 \times 10^9 M_\odot$, with several clumps of mass 10^7 - $10^8 M_\odot$ within the inner kpc radius. With even a very conservative average inflow velocity of 5 km s^{-1} , for a gas element of $10^7 M_\odot$, a mass inflow rate of $1 M_\odot \text{ yr}^{-1}$ is easily achieved. This suggests that gravitational torques from the nuclear stellar bar may produce large inflow rates ($> 1 M_\odot \text{ yr}^{-1}$) of the molecular gas.

4.7.2. Dynamical friction

Mechanisms other than gravity torques can also be important for driving gas inwards in NGC 2782. Dynamical friction (whose timescale is $\propto r^2$) becomes increasingly important at smaller radii. A body of mass M which is moving at speed v at a radius r , can be driven to the center by dynamical friction on a timescale ($t_{df} \propto (r^2 v / M \ln \Lambda)$, where $\ln \Lambda$ is the Coulomb logarithm (Binney & Tremaine 1987). The molecular gas bar in NGC 2782 contains several clumps which have sizes between $2''$ - $3''$, masses $\sim (10^7 - 10^8) M_\odot$ (for $\chi_1 = 1$), and are located within a radius of $4''$ (700 pc). The dynamical mass within a radius of $4''$ is $\sim 7.5 \times 10^9 M_\odot$ (for $i_{co} = 30$ deg), and significantly exceeds the mass of molecular gas. Therefore, if the gas clumps are self-gravitating entities, they can experience a significant drag due to dynamical friction from the stellar background. For $M \sim 10^8 M_\odot$, $r \sim 700$ pc, a rotational speed $v \sim 220 \text{ km s}^{-1}$ (derived from the CO velocity field for $i_{co} = 30$ deg), $t_{df} \sim 5 \times 10^7$ years. At smaller radii, the dynamical friction timescale drops sharply. For a conservative dynamical friction timescale of $\sim 5 \times 10^7$ years, and a total gas mass in the form of clumps of $\sim (5 \times 10^8 M_\odot)$, the average gas inflow rate is $\sim 10 M_\odot \text{ yr}^{-1}$. However, this estimate should be taken with caution. The sizes of the clumps ($2'' - 3''$) are comparable to the resolution ($\sim 2''$) of our CO observations, and it is therefore possible that each clump is made up of several smaller, less massive sub-clumps that we cannot presently resolve. With less massive clumps, the dynamical friction might only become a rapid transport mechanism at smaller radii.

4.7.3. Circumnuclear Evolution

The short dynamical timescale of $\sim 4 \times 10^6$ years (Boer et al. 1992) for the starburst-driven outflow, and the collimated H α bubble morphology with a closed shell at the edge of the bubble (Jogee et al. 1998), suggest that the outflow and starburst are probably less than 10^7 years old. How long can the central starburst in the inner 200 pc radius be sustained? The SFR is ~ 3 - $6 M_\odot \text{ yr}^{-1}$ in the central starburst, but is relatively low (1 - $2 M_\odot \text{ yr}^{-1}$) in the CO lobes which contain most of the circumnuclear molecular gas. Even in the limiting case where all of the $2.4 \times 10^9 M_\odot$ of molecular gas in the CO lobes is fed into the central starburst, it can only be sustained for $\sim 5 \times 10^8$ years. In practice, the lifetime might be even shorter since some of the gas in the lobes gets converted into stars before reaching the starburst region, and part of the interstellar medium might be blown out by the starburst-driven wind. In Paper I, we estimated that the outflow contains $\sim 10^5 M_\odot$ of hot and warm ionised gas, and possibly $\sim 2 \times 10^7 M_\odot$ of cold gas.

What about the nuclear stellar bar? Simulations show that as a nuclear stellar bar drives gas into the inner few hundred pc, it may be destroyed and even evolve into a tri-axial bulge (e.g., Friedli & Martinet 1993). Any existing large-scale primary stellar bar may be weakened or completely destroyed (Hasan & Norman 1990; Friedli & Benz 1995; Norman, Sellwood, & Hasan 1996). The destruction of the stellar bars is caused by the development of chaotic orbits and an increased mass concentration in the region of x_2 stellar orbits which are perpendicular to the bar. Typically, bar dissolution occurs if the mass concentration in

the central 200 pc radius is ≥ 1 - 2 % of the total stellar mass in the disk. The nuclear stellar bar dissolves over a few rotation periods, typically a few $\times 10^8$ years (Friedli & Martinet 1993; Combes 1994). In NGC 2782, for a standard CO-H $_2$ conversion factor, the gas mass ($2.5 \times 10^9 M_\odot$) in the CO lobes is ~ 1 % of the total stellar mass in the optical disk of radius $1'$ (10 kpc). Thus, if most of this gas is driven into the inner 200 pc radius, the nuclear stellar bar and the large-scale stellar oval can be rapidly destroyed. Nuclear stellar bars are also expected to be short-lived as a result of the rapid transfer of angular momentum from the bar to the galactic halo via dynamical friction, on timescales of a few rotation periods (Weinberg 1985), or a few $\times 10^8$ years.

4.8. Forming nuclear bars : Comparison with simulations and data

Simulations have suggested different ways of forming nuclear stellar and gas bars. Some studies have focused on gas-rich systems where the circumnuclear gas mass fraction is between 20 to 50 % (Shlosman et al. 1989; Heller & Shlosman 1994). Typically, a circumnuclear gas-rich disk forms, it becomes bar-unstable, and the nuclear gas bar rapidly fragments. However, nuclear stellar bars do not form in these simulations. This characteristic is consistent with the simulations and analytical work of Shlosman & Noguchi (1993) who find that for a disk with a gas mass fraction well above 10 %, the gas becomes clumpy, and dynamical friction between the gas clumps and the sea of stars heats up the stellar disk over several rotation periods. This results in a hot stellar disk which is stable against bar instabilities.

More relevant for NGC 2782 might be the simulations of Friedli & Martinet (1993) or Combes (1994), which produce nuclear stellar bars in moderately gas-rich circumnuclear regions. A nuclear stellar bar which is rotating faster than the large-scale primary stellar bar can form if the mass density contrast between the inner and outer regions of the primary bar is large enough. Molecular gas is critical for the decoupling : it helps to increase the central mass concentration and it loses angular momentum to the nuclear stellar bar, thereby helping it to maintain a large pattern speed. The molecular gas distribution becomes bar-like and this nuclear gas bar leads the nuclear stellar bar by a small angle, and can make up ~ 10 % of the dynamical mass. NGC 2782 has many properties consistent with these simulations: it hosts a clumpy bar-like CO feature whose radius ($7.5''$ or 1.3 kpc) is comparable to that of the nuclear stellar bar; the CO peaks lie on the leading edges of the nuclear stellar bar and show weak bar-like streaming motions; the molecular gas makes up ~ 7.5 % of the dynamical mass within a $7.5''$ (1.3 kpc) radius for a standard CO-H $_2$ conversion factor. However, one feature not so evident in these simulations, but particularly striking in NGC 2782, is the clumpiness of the molecular gas bar (Fig. 5a). If these clumps are self-gravitating entities, then dynamical friction (§ 4.7.2) might be at least as important as gravitational torques in driving the gas towards the center.

Simulations by Shaw et al. (1993) also produce a nuclear stellar bar, but it is still coupled to the primary stellar bar. In this scenario, a gas ring near the ILRs is phase-shifted in a *leading sense* with respect to the large-scale primary

stellar bar, and the gravitational perturbation of the gas on the stellar orbits produces isophotal twists. The distorted isophotes can give the appearance of a nuclear stellar bar which *always leads* the primary bar. This contrasts with the dynamically decoupled nuclear stellar bar and gaseous bar which can lead the primary bar part of the time and *trail* it at other times. In the case of NGC 2782, the nuclear stellar and gas bars are nested in a large-scale stellar oval of radius $25''$ (4.3 kpc) which could be primary stellar bar (§ 4.1). The clumpy nuclear gas bar with a PA between 70 to 85 deg, trails the large-scale stellar oval whose PA lies between 20 to 30 deg. Hence, if the large-scale stellar oval is a primary bar, then NGC 2782 supports the scenarios to form decoupled nuclear bars.

However, the simulations discussed so far deal with isolated galaxies where a spontaneously-induced primary bar was the main way to drive gas from the outer disk to the inner kpc. In the case of NGC 2782, which has experienced a recent interaction or merger (Smith 1994), such gas inflows can result from the interaction itself, namely direct tidal torques (Hernquist & Mihos 1995), as well as gravitational torques from tidally-induced large-scale stellar bars (Noguchi 1988; Combes et al. 1990; Barnes & Hernquist 1996). Once gas reaches the circumnuclear region, the formation of nuclear bars may ensue in a fashion qualitatively similar to the scenarios for isolated galaxies. Another alternative for interacting galaxies is that a nuclear stellar bar may form by the accretion of a rapidly rotating gas-rich companion. In fact, decoupled nuclear stellar disks/bars are quite common in HST images (Barth et al. 1995), and in spectroscopic studies by Rubin et al. (1997) who find that $\sim 20\%$ of a sample of 80 Virgo cluster galaxies host a decoupled disk or ring within a 500 pc radius.

We also suggest that NGC 2782 would not harbor a nuclear stellar bar if it had undergone a major merger. Violent relaxation, which operate in major mergers, tends to eradicate non-axisymmetric structures and produce an $r^{1/4}$ stellar surface brightness profile. The large gas inflow rates and large central gas concentrations typical of major mergers can rapidly destroy primary and nuclear stellar bars, as described in § 4.7.3. The large gas mass fraction also leads to the formation of gas clumps which heat the stellar component via dynamical friction, thereby making it stable against bar formation (Shlosman & Noguchi 1993). For instance, the major merger NGC 7252 has an $r^{1/4}$ K-band profile (Schweizer 1982) and the molecular gas mass fraction exceeds 30 % in the central kpc. In contrast, NGC 2782 has a molecular gas mass fraction of $\sim 8\%$ in the inner kpc radius. It has properties inconsistent with a major merger: its optical disk can be fitted with an exponential surface brightness profile, rather than an $r^{1/4}$ profile between radii of $\sim 30''$ to $60''$; its large-scale HI properties have been modeled with an intermediate (1:4) mass ratio interaction or merger by Smith (1994). Furthermore, our R-band image overlaid on the HI map in Fig. 10b shows that to the west, the stellar tail is shorter than the 50 kpc long HI tail, while to the east the opposite is true. This opposite offset in tails on different sides of a galaxy is not observed in major mergers such as NGC 7552.

5. SUMMARY AND CONCLUSIONS

We have presented a study of the peculiar interacting starburst galaxy NGC 2782 (Arp 215) based on high resolution ($2''$) interferometric OVRO CO ($J=1\rightarrow 0$) data, optical BVR and H α observations from the WIYN telescope, along with available NIR images, a 5 GHz RC map, and archival HST images. The optical and NIR data reveal a nuclear stellar bar of radius $\sim 7.5''$ (1.3 kpc) nested within a large-scale stellar oval of radius $25''$ (4.3 kpc), whose dust lane morphology suggest it might be a large-scale stellar bar. The CO maps show a clumpy, double-peaked bar-like CO feature which is offset in a leading sense with respect to the nuclear stellar bar, and has a similar radius (1.3 kpc). The CO bar contains $2.5 \times 10^9 M_\odot$ of molecular gas, assuming a standard CO-H $_2$ conversion factor and solar metallicity. The molecular gas makes up $\sim 8\%$ of the total dynamical mass within the radius (1.3 kpc) of the nuclear stellar bar. Within the CO bar, the CO emission peaks away from the nucleus, in two clumpy lobes lying on opposite sides of the nucleus, separated by $\sim 6''$ (1 kpc). The molecular gas bar is forming stars at a rate of 4 to $8 M_\odot \text{ yr}^{-1}$. Most of the star formation is centrally concentrated between the two CO lobes, in the inner 200 pc radius where the SFR is 3 to $6 M_\odot \text{ yr}^{-1}$. This intense central activity, comparable to that in the prototypical starburst M82, suggests that molecular gas fuel must have been recently present in the inner 200 pc radius. The two CO lobes lie on the leading edges of the nuclear stellar bar where gas is expected to lose angular momentum and flow inwards as a result of gravitational torques. Furthermore, while circular motions dominate the CO velocity field, the CO lobes show weak bar-like streaming motions suggestive of gas inflow. We estimate semi-analytically the gravitational torque by the nuclear stellar bar on the gas in the lobes, and our results suggest large gas inflow rates ($> 1 M_\odot \text{ yr}^{-1}$).

While there is mounting evidence from NIR surveys that many galaxies have nuclear stellar bars, the observations presented here are amongst the first ones to catch a nuclear stellar bar ‘red-handed’ in the act of feeding molecular gas into an M82-class central starburst. These observations are consistent with some theories and simulations which suggest that nuclear bars provide a powerful way to drive gas closer to the center to fuel a central starburst/AGN. In addition, we note that several massive clumps ($10^7 - 10^8 M_\odot$) are present in the inner 400 pc radius and dynamical friction might produce further gas inflow. We suggest that as a result of star formation and gas inflow, the central activity, the nuclear gas bar, and perhaps even the nuclear stellar bar, will be very short-lived and likely disappear within 5×10^8 years. The short lifetime suggests that nuclear bars can cause a rapid increase in central mass concentration, trigger intense short-lived central activity, and play an important part in circumnuclear evolution.

6. ACKNOWLEDGMENTS

Support for this work was generously provided by an AAUWEF Fellowship, NSF grant AST 96-13717, a grant from the K. T. and E. L. Norris Foundation, a Grant-in-Aid of Research from Sigma Xi (The Scientific Research Society), and a Zonta International Amelia Earhart Fellowship. We thank C. Engelbracht for generously giv-

ing us the NIR images of NGC 2782 prior to publication, and D. J. Saikia and A. Pedlar for kindly providing the 5 GHz RC maps. We thank Richard B. Larson, F. Combes, J. Sellwood, and the participants of the 1996

Summer school on “Starbursts: Triggers, Nature and Evolution” at Les Houches for useful discussions. We thank Jeannette Barnes at NOAO for helping in the production of solitaires.

REFERENCES

- Aalto, S., Booth, R. S., Black, J. H., & Johansson, L. E. B. 1995, *A&A*, 300, 369.
- Athanassoula, E. 1992, *MNRAS*, 259, 345
- Balick, B., & Heckman, T. 1981, *A&A*, 96, 271
- Balzano, V. A. 1983, *ApJ*, 268, 602
- Barnes, J. E., & Hernquist, L. 1996, *ApJ*, 471, 115
- Barth, A. J., Ho L. C., Filippenko, A. V., Sargent, W. L. 1995, *AJ*, 110
- Binney, J., & Tremaine, S. 1987, *Galactic Dynamics*, ed. Ostriker, J. P. (Princeton, N. J.: Princeton University Press)
- Boer, B., Schulz, H., & Keel, W. C. 1992, *A&A*, 260, 67
- Buta, R., & Crocker, D. A. 1993, *AJ*, 105, 1344
- Bryant, P. M. & Scoville, N. Z. 1999, *AJ*, 117, in press
- Byrd, G., Rautiainen, P., Salo, H., Buta, R., & Crocher, D. A. 1994, *AJ*, 108, 476
- Combes, F., & Gerin, M. 1985, *A&A*, 150, 327
- Combes, F., Debasch, F., Friedli, D., & Pfenniger, D. 1990, *A&A*, 233, 82
- Combes, F. 1994, in *Mass-Transfer Induced Activity in Galaxies*, ed. Shlosman, I. (Cambridge University Press), 170
- de Vaucouleurs, G., de Vaucouleurs, A., Corwin Jr., H. G., Buta, R. J., Paturel, G., & Fouque, P. 1991, *Third Reference Catalogue of Bright Galaxies* (New York: Springer) (RC3)
- de Vaucouleurs, A., & Longo, G. 1988, “Catalogue of Visual and Infrared Photometry of Galaxies from 0.5 micrometer to 10 micrometer (1961-1985)”, University of Texas Monographs in Astronomy (Austin: University of Texas)
- Devereux, N. A. 1989, *ApJ*, 346, 126
- Elmegreen, D. M., Elmegreen, B. G., Chromey, F. R., Hasselbacher, D. A., & Bissell B. A. 1996, *AJ*, 111, 1880
- Engelbracht, C. W., Rieke, M. J., & Rieke, G. H. 1999, in preparation
- Evans, A. S., Mazzarella, J. M., Surace, J. A., & Sanders, D. B. 1999 *ApJ*, 511, 731
- Evans, I. N., Koratkar, A. P., Storchi-Bergmann, T., Kirkpatrick, H., Heckman, T. M., & Wilson, S. A. 1996, *ApJS*, 185, 93
- Evans, A. S., Surace, J. A., & Mazzarella, J. M. 1999, in preparation
- Forbes, D. A., Ward, M. J., DePoy, D. L., Boisson, C., & Smith, M. S. 1992, *MNRAS*, 254, 519
- Friedli, D., & Martinet, L. 1993, *A&A*, 277, 27
- Friedli, D. & Benz, W. 1995, *A&A*, 301, 649
- Friedli, D., Wozniak, H., Rieke, M., & Bratschi, P. 1996, *A&AS*, 118, 461
- Garcia-Burillo, Sempere, M. J., Combes, F., & Neri, R. 1998, *A&A*, 333, 864
- Guiricin, G., Tamburni, L., Mardirossin, F., Mezzetti, M., & Monaco, P. 1994, *ApJ*, 427, 202
- Hasan, H., & Norman, C. 1990, *ApJ*, 361, 69
- Helfer, T. T., & Blitz, L., 1993, *ApJ*, 419, 86
- Heller, C. H., & Shlosman, I. 1994, *ApJ*, 424, 84
- Hernquist, L., & Mihos, J. C. 1995, *ApJ*, 448, 41
- Hodge, P. W., & Kennicutt, R. C. 1983, *ApJ*, 268, L75
- Hunter, D. A., Gillett, F. C., Gallagher, J. S., Rice, W. L., & Low, F. J. 1986, *ApJ*, 303, 171.
- Hurt, R. L., & Turner, J. L. 1991, *ApJ*, 377, 434
- Irwin, J. A., & Sofue, Y. 1992, *ApJ*, 396, L75
- Ishizuki, S., Kawabe, R., Ishiguro, M., Okumura, S. K., & Morita, K.-I., 1990, *Nature*, 344, 224
- Ishuzuki, S. 1994, in *Proceedings of IAU Colloquium 140, Astronomy with Millimeter and Submillimeter Wave Interferometry*, eds. Ishiguro, M., & Welch, J. M. (ASP Conference Series), 292
- Jackson, J. M., & Ho, P. T. P. 1988, *ApJ*, 324, L5
- Jogee, S., Kenney, J. D. P. & Smith B. J., 1998, *ApJL*, 494, L185 (**Paper I**)
- Jogee, S. 1998, Ph. D. Thesis, Yale University.
- Jogee, S., & Kenney, J. D. P. 1998, *Proceedings of IAU Symposium No. 184, The Central Regions of the Galaxy and Galaxies*, ed. Y. Sofue (Dordrecht: Kluwer Academic Publishers)
- Jungwiert, B., Combes, F., & Axon, D. J. 1997, *A&AS*, 125, 479
- Kenney, J. D. P., & Young, J. S. 1989, *ApJ*, 344, 171.
- Kenney, J. D. P., Wilson, C. D., Scoville, N. Z., Devereux, N. A., & Young, J. S. 1992, *ApJ*, 395, 179
- Kennicutt, R. C., Jr. 1983, *ApJ*, 272, 54
- Kennicutt, R. C., Jr., Keel, W. C., & Blaha, C. A. 1989, *AJ*, 97, 1022
- Kinney, A. L., Bregman, J. N., Huggins, P. T., Glassgold, A. E., & Cohen, R. D. 1984, *PASP*, 96, 398
- Knapen, J. H., Beckman, J. E., Shlosman, I., Peletier, R. F., Heller, C. H., & de Jong, R. S. 1995a, *ApJL*, 443, L73.
- Knapen, J. H., Beckman, J. E., Heller, C. H., Shlosman, I., & De Jong, R. S. 1995b, *ApJ*, 454, 623
- Mihalas, D., & Binney, J. 1981, *Galactic Astronomy* (New York: W. H. Freeman and Company)
- Mihos, J. C., & Hernquist, L. 1994, *ApJ*, 425, L13
- Negroponte, J., & White, S. D. M. 1983, *MNRAS*, 205, 1009
- Noguchi, M. 1988, *A&A*, 203, 259
- Norman, C. A., Sellwood, J. A., & Hasan, H. 1996, *ApJ*, 462, 114.
- Padin, S., Scott, S. L., Woody, D. P., Scoville, N. Z., Seling, T. V., Finch, R. P., Giovanine, C. J., & Lawrence, R. P. 1991, *PASP*, 103, 461
- Pierce, J. M., & Tully, R. B. 1988, *ApJ*, 330, 579
- Piner, B., Glenn, S., James, M., & Teuben, P. J. 1995, *ApJ*, 449, 508
- Pompea, S. M., & Rieke, G. M. 1990, *ApJ*, 356, 416
- Puxley, P. J., Hawarden, T. G., & Mountain, C. M. 1990, *ApJ*, 364, 77.
- Quillen, A. C., Frogel, J. A., Kuchinski, L. E., Terndrup, D. M. 1995, *AJ*, 110, 156.
- Rand, R. J. 1995, *AJ*, 109, 244
- Rubin, V. C., Burstein, D., Ford, Jr., W. K., & Thonnard, N. 1985, *ApJ*, 289, 81
- Rubin, V. C., Kenney, J. D. P., Young, J. S. 1997, *AJ*, 113, 1250
- Saikia, D. J., Pedlar, A., Unger, S. W., & Axon, D. J. 1994, *MNRAS*, 270, 46
- Sakka, K., Oka, S., & Wakamatsu, K. 1973, *PASJ*, 25, 153
- Sandage, A. 1961, *The Hubble Atlas of Galaxies* (Washington D. C.: Carnegie Institute of Washington)
- Sandage, A. & Tammann, G. A. 1981, *A revised Shapley Ames Catalog of Bright Galaxies* (Washington D. C.: Carnegie Institute of Washington)
- Sandage, A. & Bedke, J., 1994, *The Carnegie Atlas of Galaxies* (Washington D. C.: Carnegie Institute of Washington)
- Schinnerer, E., Eckart, A., Quirrenbach, A., Boker, T., Tacconi-Garman, L. E., Krabbe, A., & Sternberg, A. 1997, *ApJ*, 488, 174
- Schwarz, M. P. 1984, *MNRAS*, 221, 195
- Schweizer, F. 1982, *ApJ*, 252, 455
- Scoville, N. Z., Yun, M. S., Windhorst, R. A., Keel W. C., & Armus, L. 1997, *ApJ*, 485, L21
- Scoville, N. Z., Yun, M. S., Clemens, D. P., Sanders, D. B., & Waller, W. H. 1987, *ApJS*, 63, 821
- Scoville, N. Z., & Sanders, D. B. 1987, in *Interstellar Processes*, ed. D. J. Hollenbach & H. A. Thronson (Dordrecht: Reidel), 21
- Scoville, N. Z., Carlstrom, J. E., Chandler, C. J., Phillips, J. A., Scott, S. L., Tilanus, R. P. J., & Wang, Z. 1993, *PASP*, 105, 1982
- Shaw, M. A., Combes, F., Axon, D. J., Wright, G. S., 1993, *A&A*, 273, 31
- Shlosman, I., Frank, J., & Begelman, M. C. 1989, *Nature*, 338, 45
- Shlosman, I., & Noguchi, M. 1993, *ApJ*, 414, 474
- Simkin, S. M., Su, H. J., Schwarz, M. P. 1980, *ApJ*, 237, 404
- Smith, B. J. 1994, *AJ*, 107, 1695
- Smith, B. J. 1991, *ApJ*, 378, 39
- Smith, B. J., Curtis, S., Kenney, J. D. P., & Jogee, S. 1999, *AJ*, 117, 1237
- Teuben, P. J., Sanders, R. H., Atherton, P. D., van Albada, G. D. 1986, *MNRAS*, 221, 1
- Tubb, A. D. 1982, *ApJ*, 255, 458
- Wall, W. F., & Jaffe, D. T. 1990, *ApJ*, 361, L45
- Weinberg, M. D. 1985, *MNRAS*, 213, 451.
- Wild, W., Harris, A. I., Eckart, A., Genzel, R., Graf, U. U., Jackson, J. M., Russell, A. P. G., & Stutzki, J. 1992, *A&A*, 265, 447
- Wozniak H., Friedli D., Martinet L., Martin P., Bratschi P., 1995, *A&AS* 111, 115
- Young, J. S. et al. 1995, *ApJS*, 98, 219
- Young, J. S., Claussen, M. J., Kleinmann, G. S., Rubin, V. C., & Scoville, N. Z. 1988, *ApJ*, 331, L81
- Yun, M. S., & Scoville, N. Z. 1995, *ApJ*, 451, L45

(Plate 1)– The optical morphology: The WIYN R-band image of NGC 2782 with a $6.5'$ (66 kpc) field of view reveals an optical disk which is bracketed by two stellar tails. The eastern stellar plume extends to a radius of $\sim 2.7'$ (27 kpc), while the fainter, diffuse western tail stretches out to $\sim 4'$ (40 kpc). Except for three ripples at radii of $25''$, $45''$ and $60''$, the optical disk is relatively undisturbed within a radius of $\sim 1'$ (10 kpc).

Fig. 2 – CO (J=1->0) channel maps: The naturally weighted channels show emission over $V_{lsr} = 2364$ to 2728 km s^{-1} . The velocity resolution is 10.4 km s^{-1} . The contour levels are -5, -3, 3, 5, 8, 11 times the noise level (11 mJy per beam). The synthesized beam is shown in the top panel. The cross marks the 5 GHz radio continuum peak.

Fig. 3 — The nuclear gas and stellar bars nested in a large-scale oval feature: (a) The I image with a $3'$ (30 kpc) field of view shows a relatively circular optical disk which has a radius of $\sim 1'$ (10 kpc). A weak oval feature of radius $25''$ (4.3 kpc), at a position angle (PA) of ~ 20 deg is present in the disk. It is flanked by two relatively straight dust lanes which are visible in the B and B-V images (Figs. 7a & 7b, Plate L2). The locations of the dust lanes are shown as solid lines here. The oval feature might be a weak primary stellar bar. (b) K contours (Engelbracht et al. 1997) on high resolution ($2.1'' \times 1.5''$) CO (greyscale) for a $1.5'$ (15 kpc) field of view. The dust lanes are again shown as solid lines. Within the large-scale oval of radius $25''$ (4.3 kpc), is nested a gas-rich nuclear stellar bar which has a PA of 100 deg and a radius of $\sim 7.5''$ (1.3 kpc). (c) K contours on CO greyscale for the central $20''$ (3.4 kpc) field of view only. The nuclear CO bar has a similar extent as the nuclear stellar bar and leads it by a small angle. (d) 5 GHz RC (contours, Saikia et al. 1994) on the high resolution CO (greyscale) for a central $20''$ (3.4 kpc) field of view. The molecular gas bar is associated with star formation whose intensity peaks in the inner 200 pc of the bar. The northern and southern RC bubbles are associated with the starburst outflow. The two CO spurs, labelled O1 and O2, lie inside the outflow bubbles and are elongated along the CO kinematic axis.

Fig. 4 — Isophotal analysis of the K and I images: The radial profiles of surface brightness, ellipticity and position angle of the azimuthally-averaged K and I light are shown. The profiles reveal a nuclear stellar bar which has a maximum ellipticity of 0.28, a PA of ~ 100 deg, and a radius of $\sim 7.5''$ (1.3 kpc). The ellipticity falls to a minimum at a radius of $8''$, and then smoothly rises to ~ 0.26 at a radius of $\sim 25''$, while the position angle twists gradually from a PA of 0 deg to ~ 20 deg. It is possible, but not certain, that the second smooth rise in ellipticity is indicative of a large-scale primary stellar bar. Further out, the signal-to noise in the K-band image is very low and the I-band image is used. In this image, the ellipticity appears to fall again and it reaches values below 0.1 in the outer disk at radii beyond $50''$ (8.5 kpc).

Fig. 5 — The CO intensity and velocity fields: (a) Uniformly weighted ($2.1'' \times 1.5''$) CO total intensity map of the central $20''$ (3.4 kpc). Most of the circumnuclear CO in NGC 2782 lies within a radius of $8''$ (1.4 kpc), and has a bar-like distribution. The CO emission peaks in two extended clumpy lobes which lie on opposite sides of the nucleus, separated by ~ 1 kpc. The CO bar leads the nuclear stellar bar whose PA is marked. The two faint CO spurs, labelled O1 and O2, are elongated along the kinematic minor axis. The contour levels are 5, 10, 20,...100 % of the peak flux. The cross marks the 5 GHz RC peak. (b) Uniformly weighted ($2.1'' \times 1.5''$) CO velocity field (moment 1, contours) on the CO total intensity map. Although the gas in the central $8''$ (1.4 kpc) has predominantly circular motions, there are weak bar-like streaming motions in the CO lobes, and non-circular motions in the two CO spurs.

Fig. 6 — The CO kinematics: (a) The spatial velocity plot along the major axis (75 deg) with a width of $\pm 1.0''$. The systemic velocity of 2555 km s^{-1} has been subtracted from velocities on the y-axis. Complex kinematics indicative of non-circular motions are present $1''$ to $4''$ along the eastern and western sides of the major axis. The complex gas kinematics are associated with the western and eastern CO peaks. The features marked as A1, A2, A3, and A4 delineate the large linewidths and complex kinematics at the position of these peaks. Contour levels are 20, 25, 30, 40, 50, 60, 70, 80, 90, 100 % of the peak flux (73 mJy per beam). The cross in Figs. 6a-b marks the same position as in Figure 5 at (09 10 53.65, +40 19 15.3), where the systemic velocity is 2555 km s^{-1} . (b) The spatial velocity plot along the CO kinematic minor axis with a width of $\pm 0.5''$. We can see weakly emitting gas whose velocities deviate from the systemic velocity by $\sim 50 \text{ km s}^{-1}$ near O1, and by -30 to -50 km s^{-1} near O2. This indicates non-circular motions resulting from vertical outflow out of the disk plane or/and radial gas inflow in the disk plane. Contour levels are 2.5, 3, 3.5, 4, 4.5, 5, 6, 7 times the noise level (11 mJy per beam).

Fig. 7 (Plate 2) — The CO distribution in relation to the dust lanes: (a) The WIYN B image with a $1.6'$ (16.3 kpc) field of view shows two dust lanes which are offset from the nucleus and extend out to a radius of $\sim 25''$ (4.3 kpc). The two dust lanes are relatively straight and parallel to each other. Their appearance is similar to the dust lanes observed along the leading edges of bars in many spiral galaxies. (b) Naturally weighted ($2.6'' \times 2.0''$) CO intensity (moment 0, contours) map on the WIYN B-V image (greyscale) for a $1.6'$ (16.3 kpc) field of view. The contour levels are 10, 20, ...100 % of the of the peak flux ($12.46 \text{ Jy km s}^{-1}$ per beam). Notice that the dust lanes bracket the CO bar, and the two CO peaks lie at 30 - 40 deg, rather than 90 deg, to the dust lanes. Further out, fainter streams of CO emission lie along the dust lanes. The southern CO stream suggests a loosely wound trailing spiral arm.

Fig. 8 — The HST $H\alpha$ + $[N II]$ image with a $7''$ (1.2 kpc) field of view shows the central starburst, highlights knots of HII regions in the northern arc of star formation running approximately east-west, and resolves the southern starburst-driven outflow ‘bubble’ (Jogee et al. 1998).

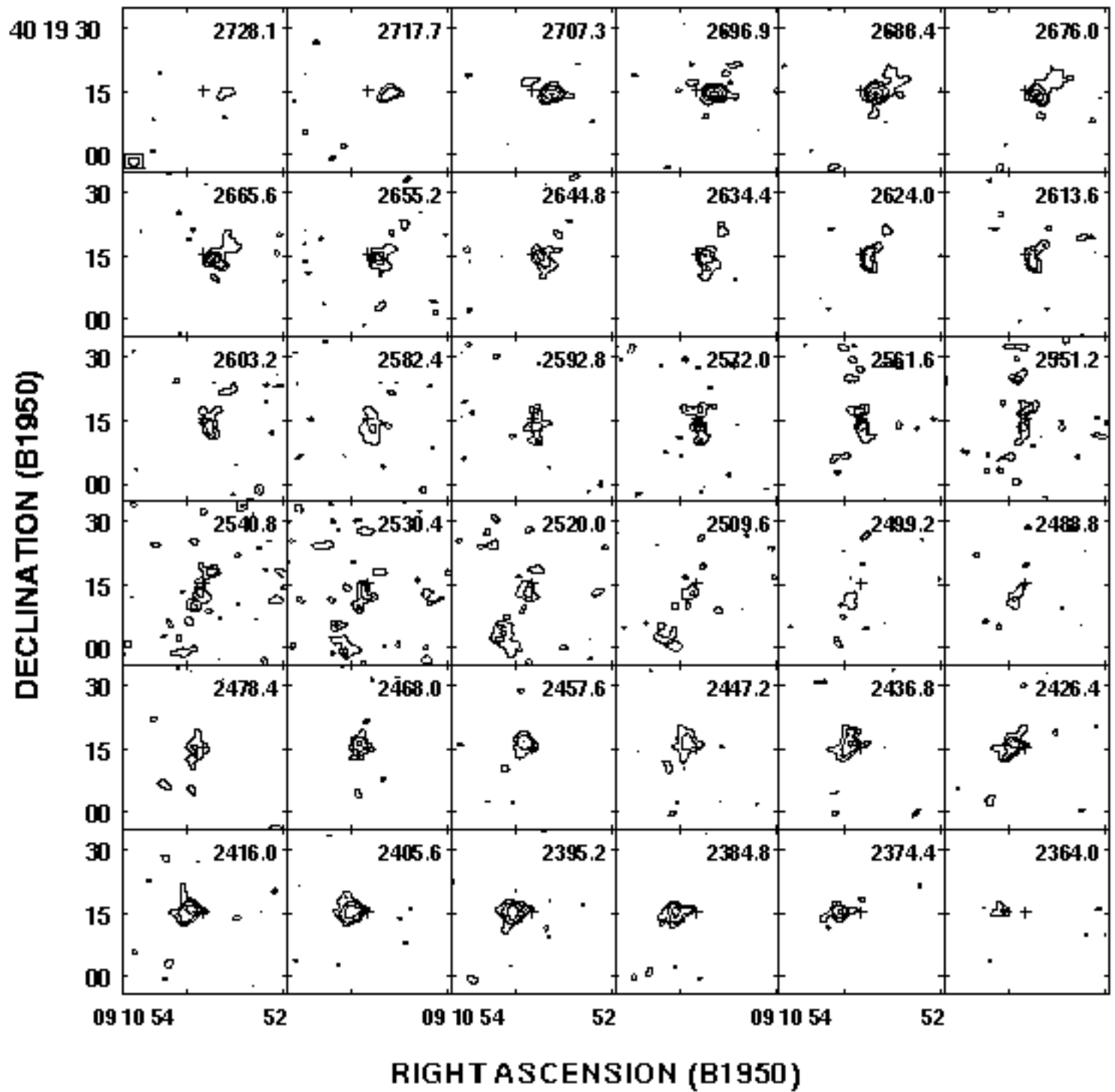
Fig. 9 (a) Top: HST V-band (F555W) image with a $35''$ (6 kpc) field of view. **(b)** Bottom: The uniformly weighted ($2.1'' \times 1.5''$ or 355×255 pc) OVRO CO map superposed on the HST V image. These images show the northern arc of star formation running approximately east-west in the inner kpc radius, and a set of dust lanes extending northeast beyond a radius of $20''$ (3.4 kpc). These dust lanes coincide with those seen in the ground-based B-V image and are offset towards the leading edge of the large-scale stellar oval. About $4''$ (680 pc) north of the nucleus, another set of striking dust lanes run approximately east-west, and are offset in a leading sense with respect to the nuclear bar-like CO feature.

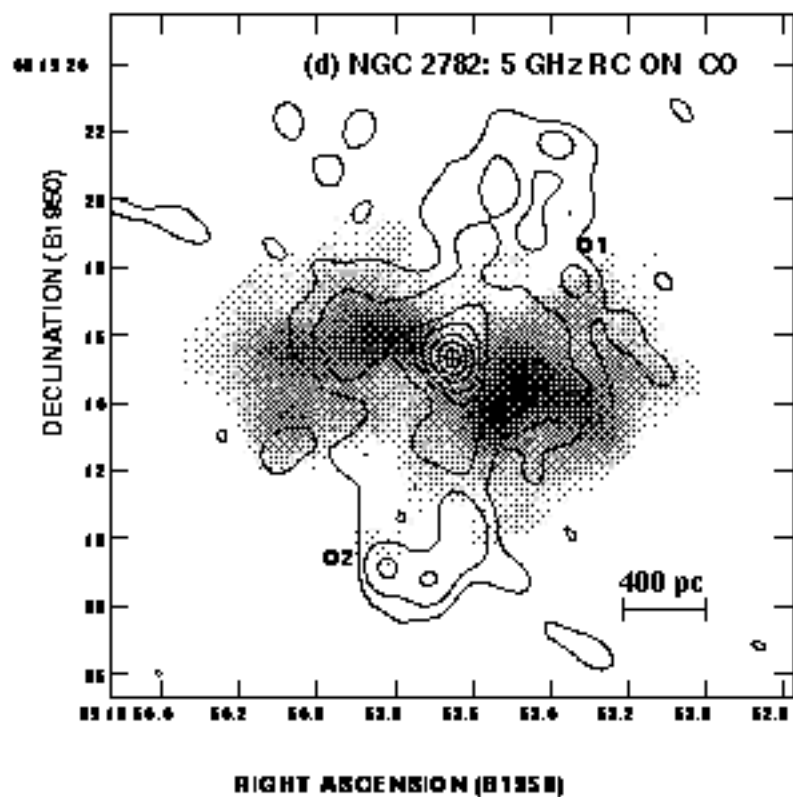
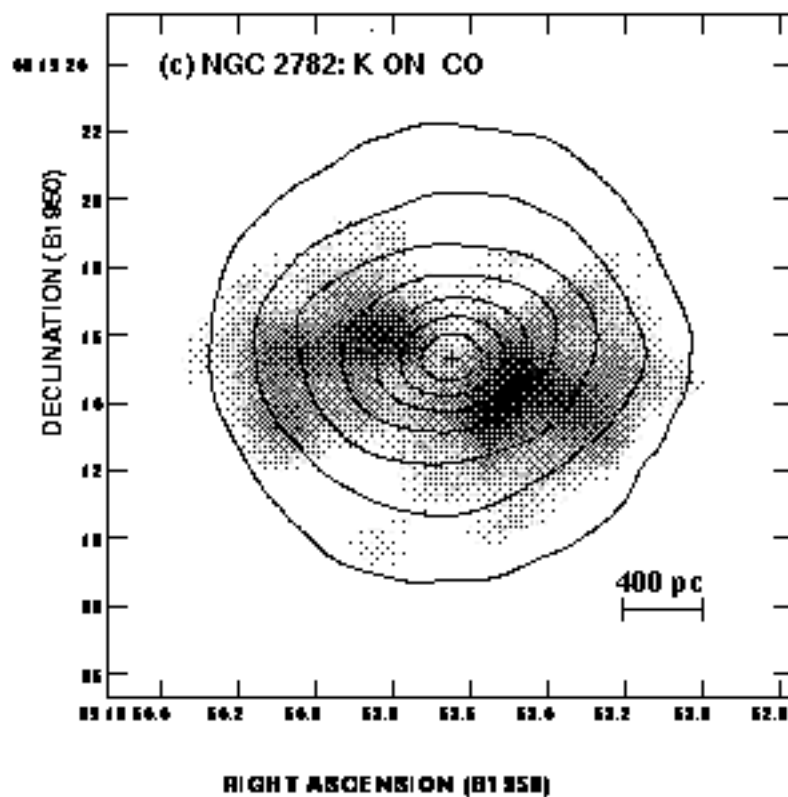
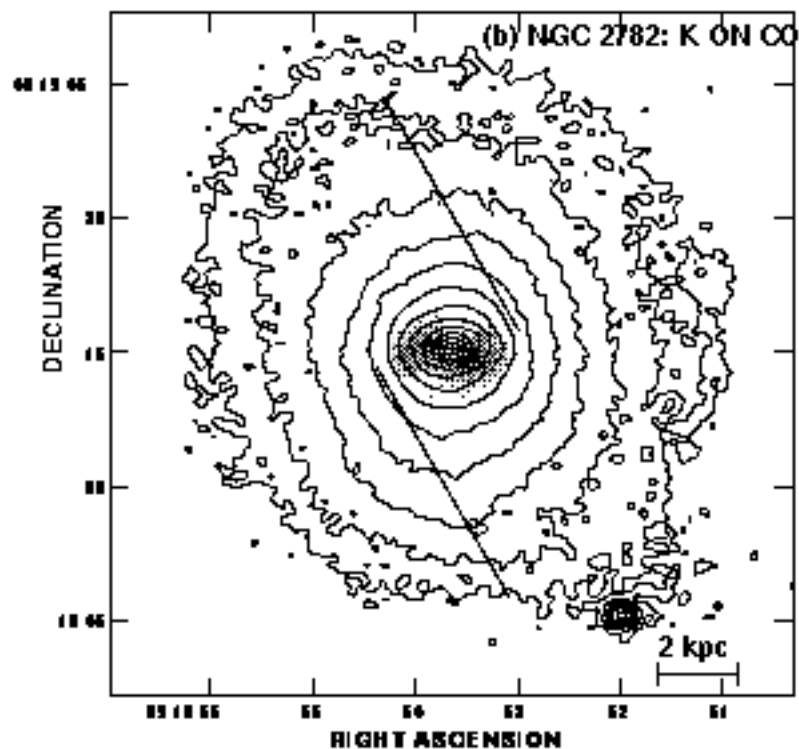
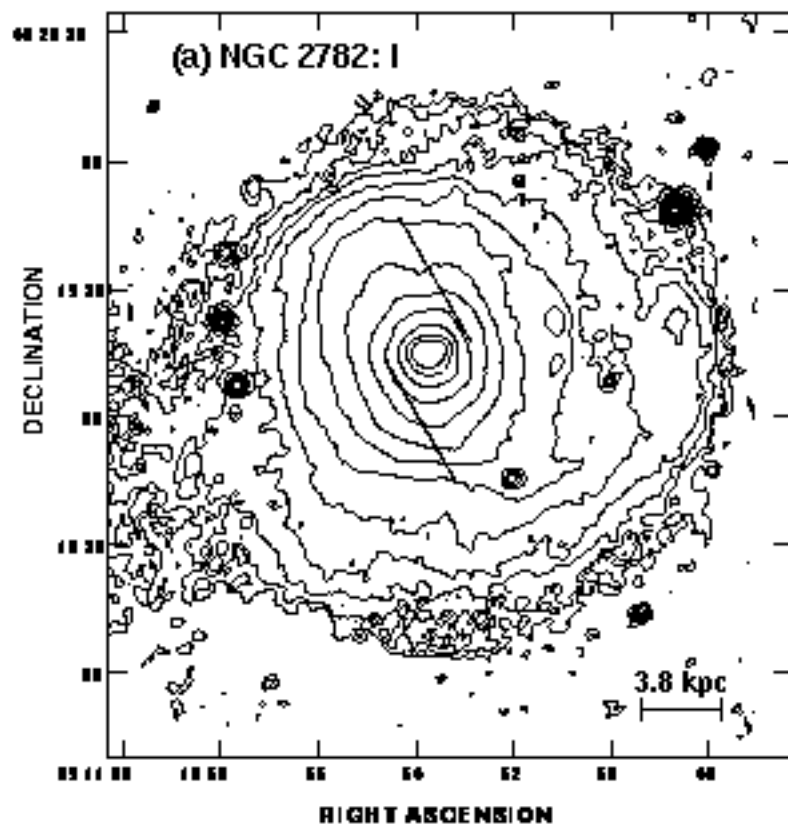
Fig.10 — Comparison of the HI and stellar distributions: **(a)** The HI map (Smith 1994) of NGC 2782 with a $6.8'$ (69 kpc) field of view reveals a blueshifted western tail, a redshifted eastern tail, and an HI disk. Levels plotted are 10, 20,...,100 % of the peak flux of $0.34 \text{ Jy km s}^{-1}$ per beam. The western tail is $5'$ (50 kpc) long and contains 40 % of the total HI mass of the galaxy. **(b)** Contours of the smoothed R image on the HI map. The eastern might be *stellar plume* extending beyond the $2'$ (20 kpc) long eastern *HI tail*. In contrast, the western diffuse *stellar tail* seems shorter than the western *HI tail* by $\sim 1'$ (10 kpc). The cross marks the 5 GHz RC peak.

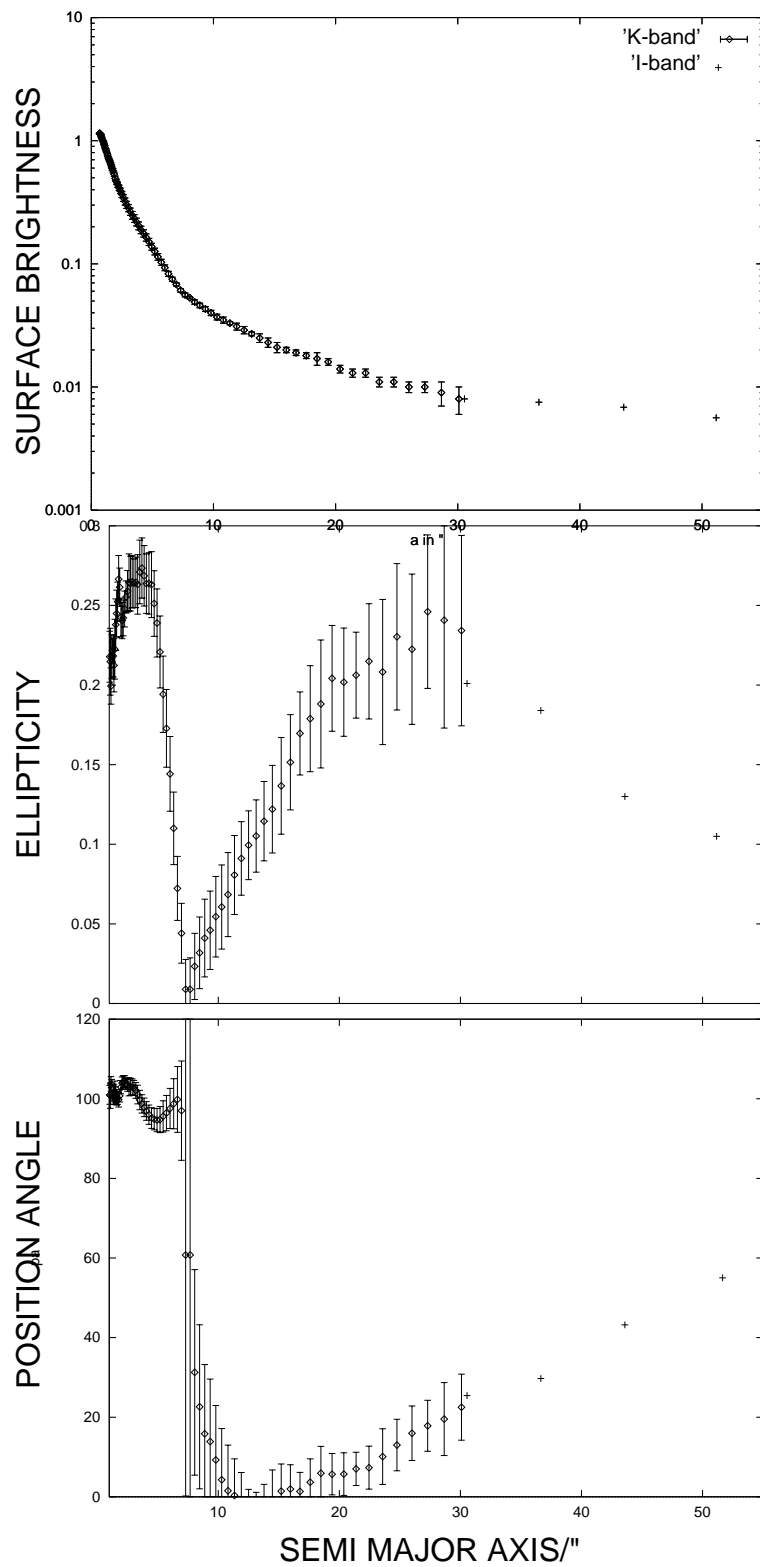
This figure "jogee-p2fig1.low.jpg" is available in "jpg" format from:

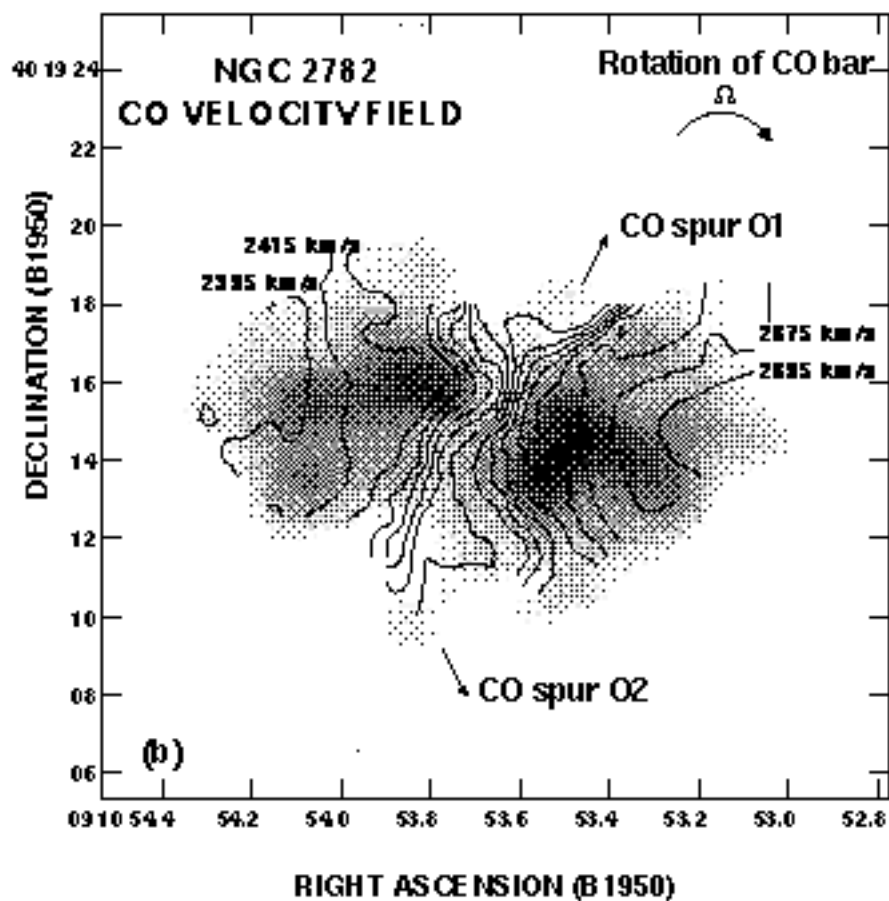
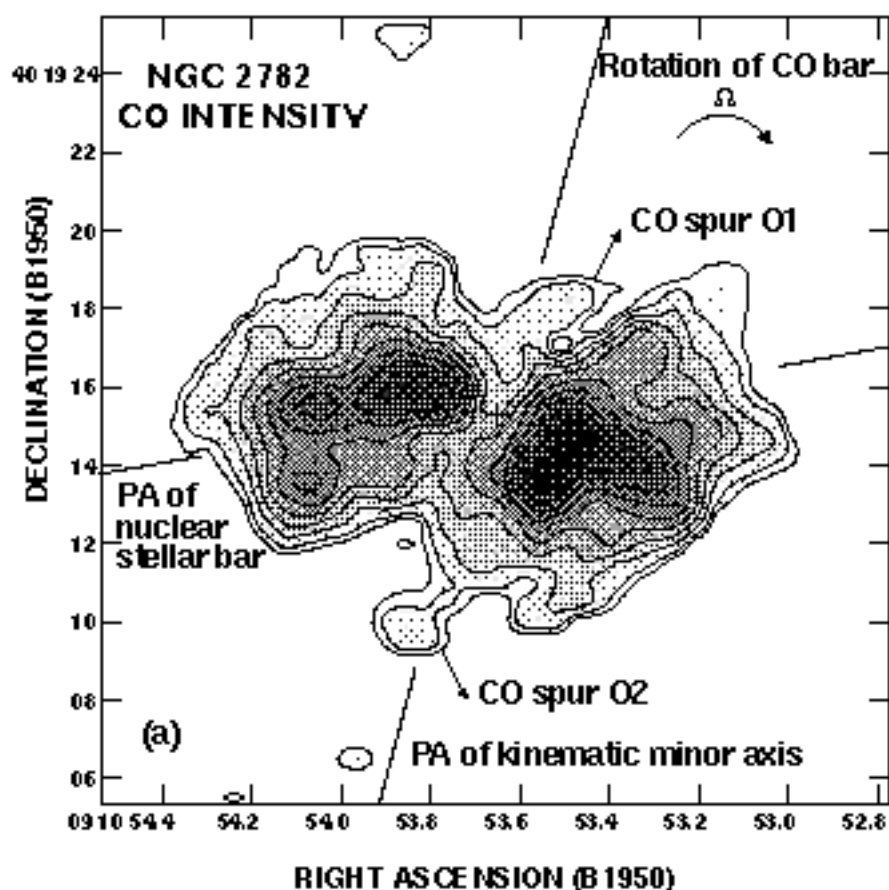
<http://arxiv.org/ps/astro-ph/9907085v1>

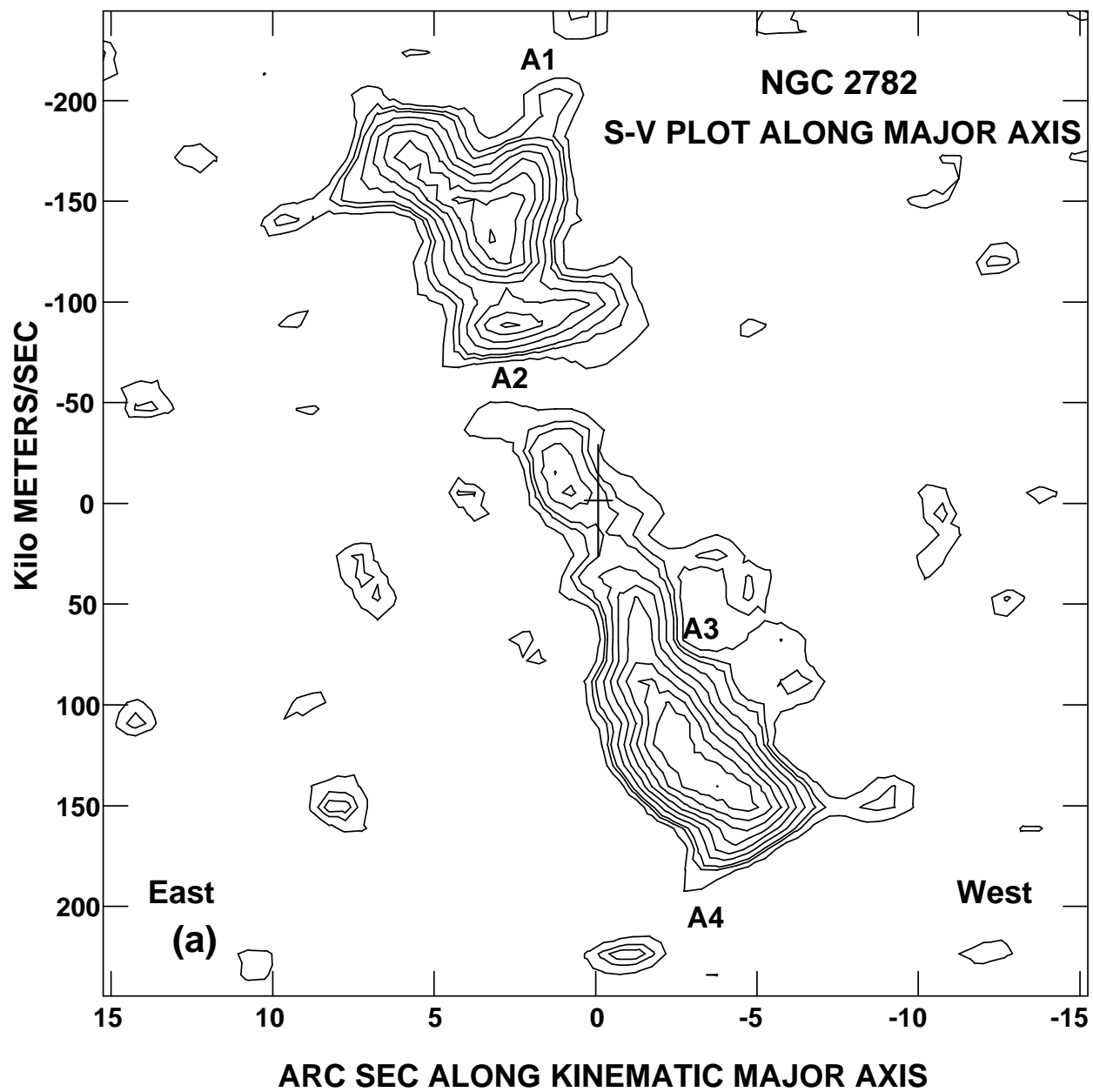
NGC 2782: CO (J=1-→0) naturally weighted channel maps

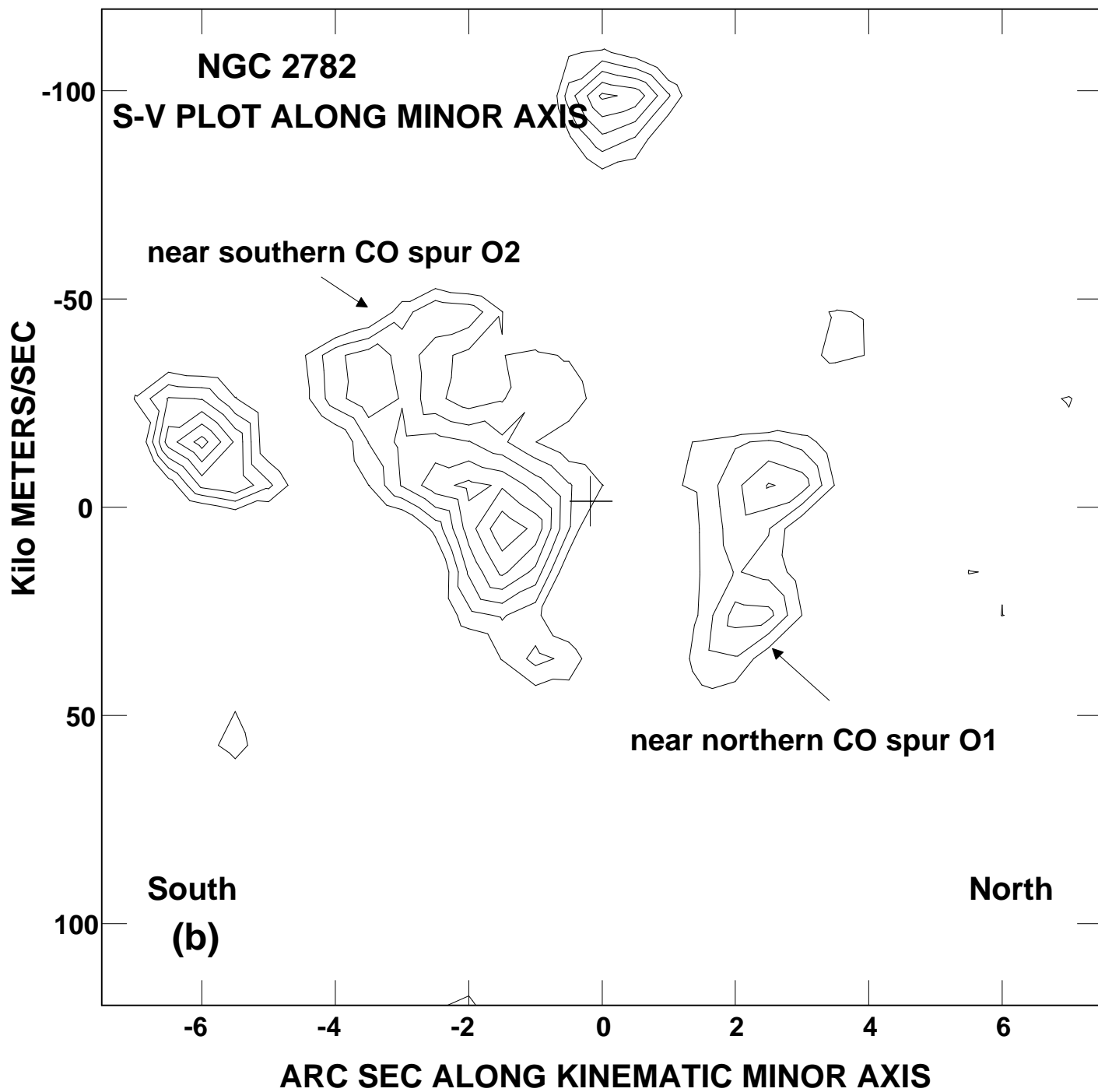








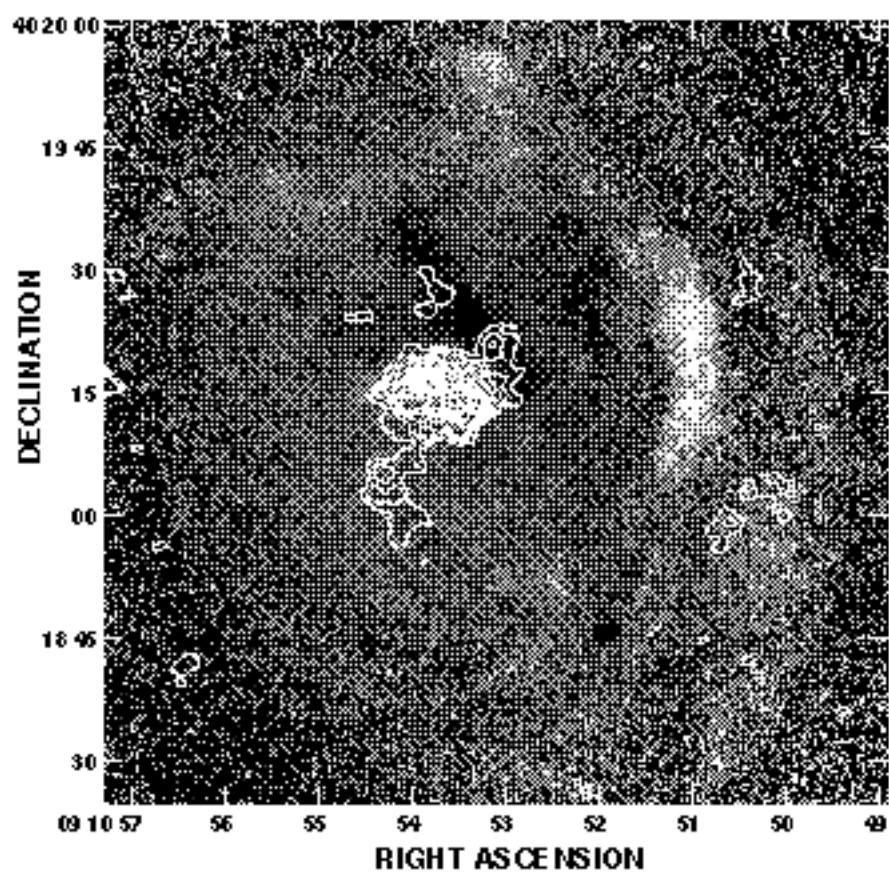


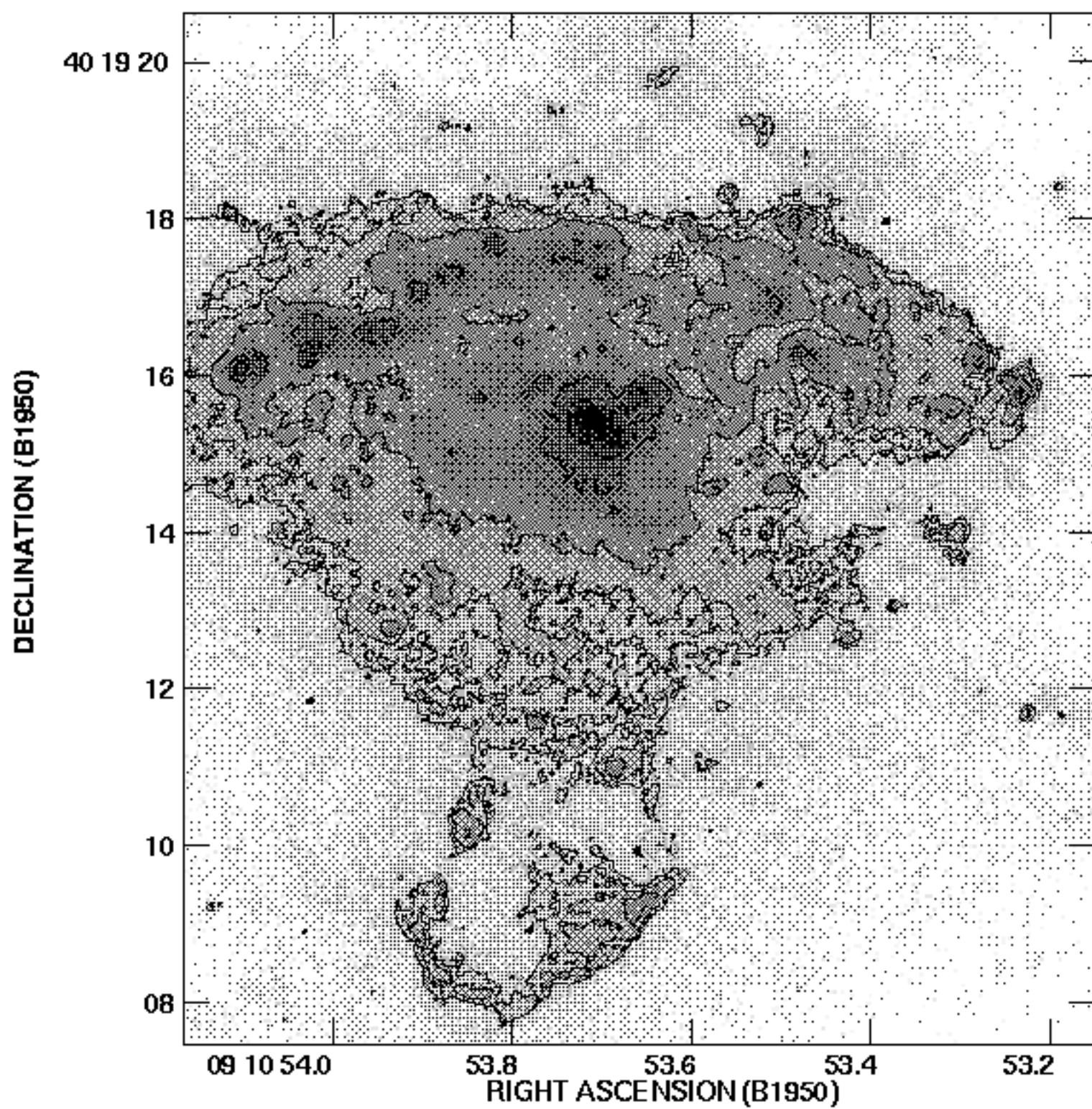


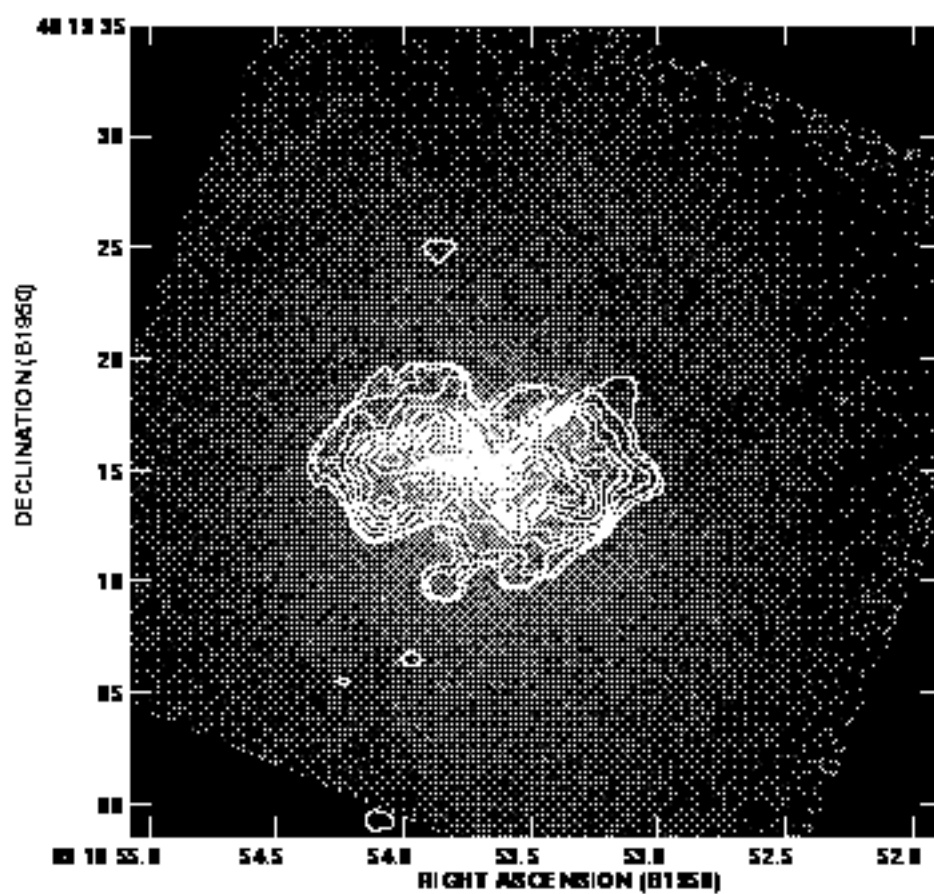
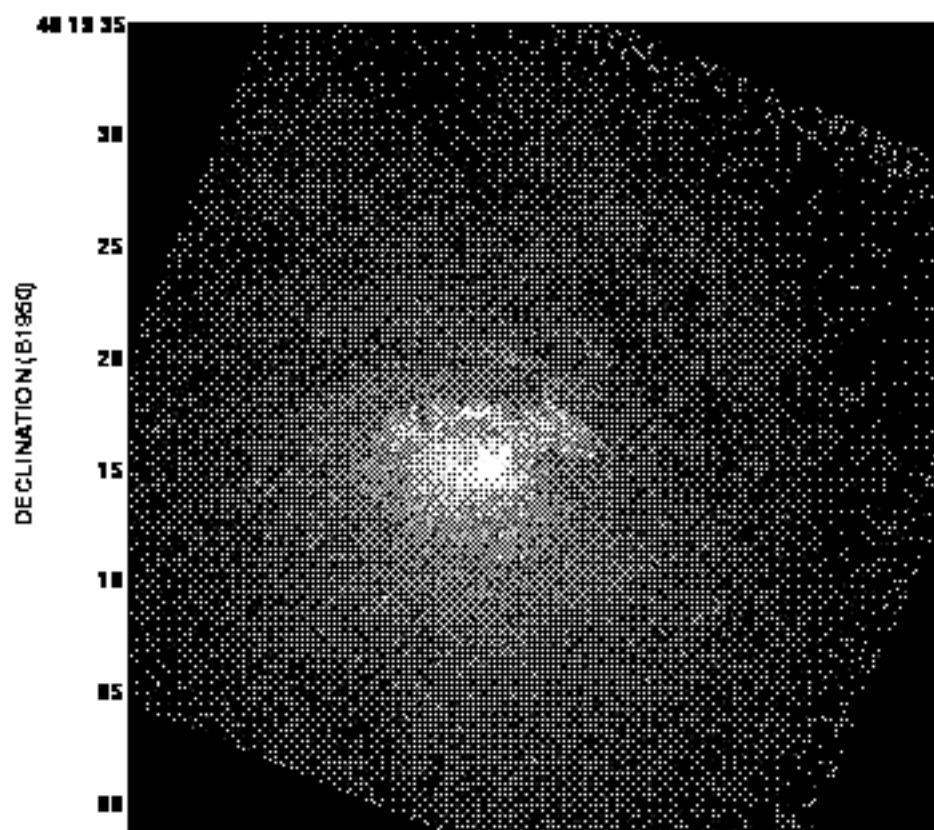
This figure "jogee-p2fig7a.low.jpg" is available in "jpg" format from:

<http://arxiv.org/ps/astro-ph/9907085v1>

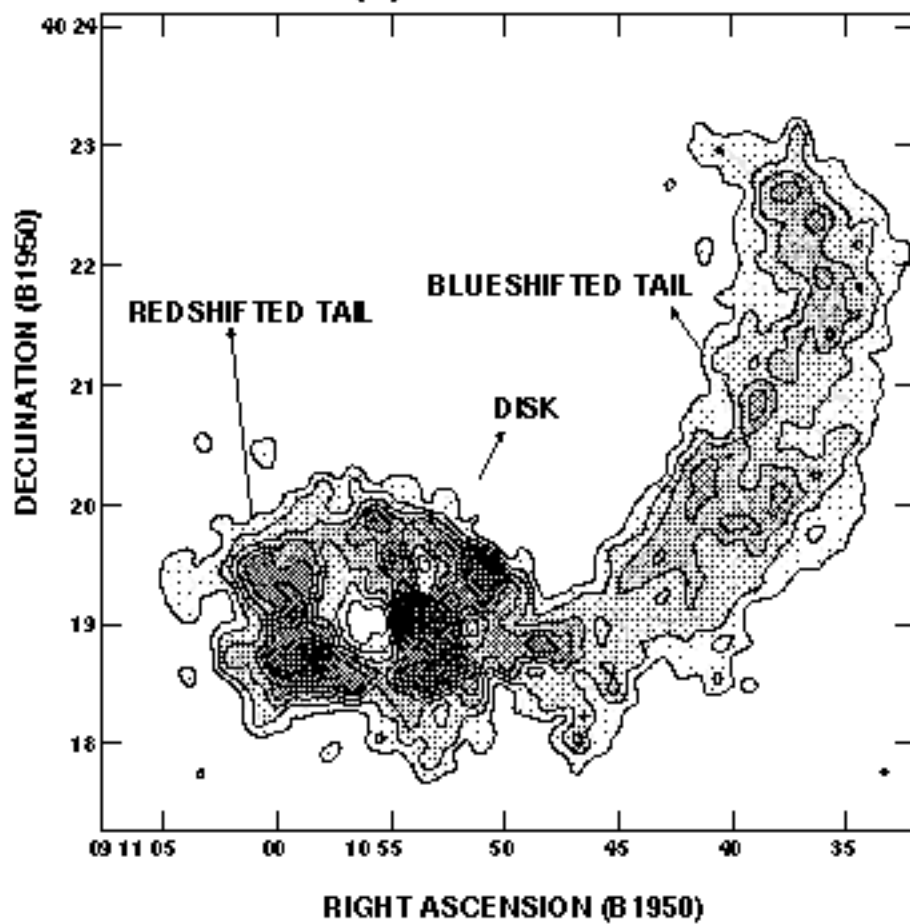
NGC 2782: CO CONTOURS ON B-V GREYSCALE







(a) NGC 2782 : HI



(b) NGC 2782 : R CONTOURS ON HI GREYSCALE

